Chapter 4
Heat Transfer in Single-Phase Flows

The subject of this chapter is single-phase heat transfer in micro-channels. Several aspects of the problem are considered in the frame of a continuum model, corresponding to small Knudsen number. A number of special problems of the theory of heat transfer in micro-channels, such as the effect of viscous energy dissipation, axial heat conduction, heat transfer characteristics of gaseous flows in micro-channels, and electro-osmotic heat transfer in micro-channels, are also discussed in this chapter.

4.1 Introduction

Heat transfer in straight tubes and channels has been the subject of much research for the last century. Theoretical predictions in this field agree fairly well with known experimental data related to heat transfer in the conventional size channels (cf. Petukhov 1967; Kays and Crawford 1993; Baehr and Stephan 1998; Schlichting 2000). The development of micro-mechanics during the last decades stimulated a great interest in heat transfer studies in micro-channels (cf. Ho and Tai 1998; Gad-el-Hak 1999). A number of theoretical and experimental investigations devoted to this problem were performed from 1994 to 2006, including Wang and Peng (1994), Peng and Peterson (1995), Peng et al. (1995), Peng and Peterson (1996), Ma and Peterson (1997), Mala et al. (1997a,b), Mala and Li (1999), Qu et al. (2000), Qu and Mudawar (2002a,b), Gao et al. (2002), Zhao and Lu (2002), Wu and Cheng (2003), Weigand and Lauffer (2004), Male et al. (2004), Lelea et al. (2004), Gamart et al. (2005), Reynaud et al. (2005), Lelea (2005), and Yoo (2006). Data on heat transfer in laminar and turbulent flows in micro-channels of different geometry were obtained. Several special problems related to heat transfer in micro-channels were discussed, including the effect of axial conduction in the wall and viscous dissipation effect (Tso and Mahulikar 1998; Tso and Mahulikar 1999; Tso and Mahulikar 2000; Tunc and Bayazitoglu 2001; Koo and Kleinstreuer 2004; Maran-

© Springer 2009

zana et al. 2004). Comprehensive surveys may be found in Bailey et al. (1995), Sobhan and Garimella (2001), Kandlikar and Grande (2002), Gua and Li (2003), Garimella and Sobhan (2003), Celata et al. (2004), Hassan et al. (2004), and Morini (2004).

We note that different methods of heating are used by various researchers, as shown in Fig. 4.1.

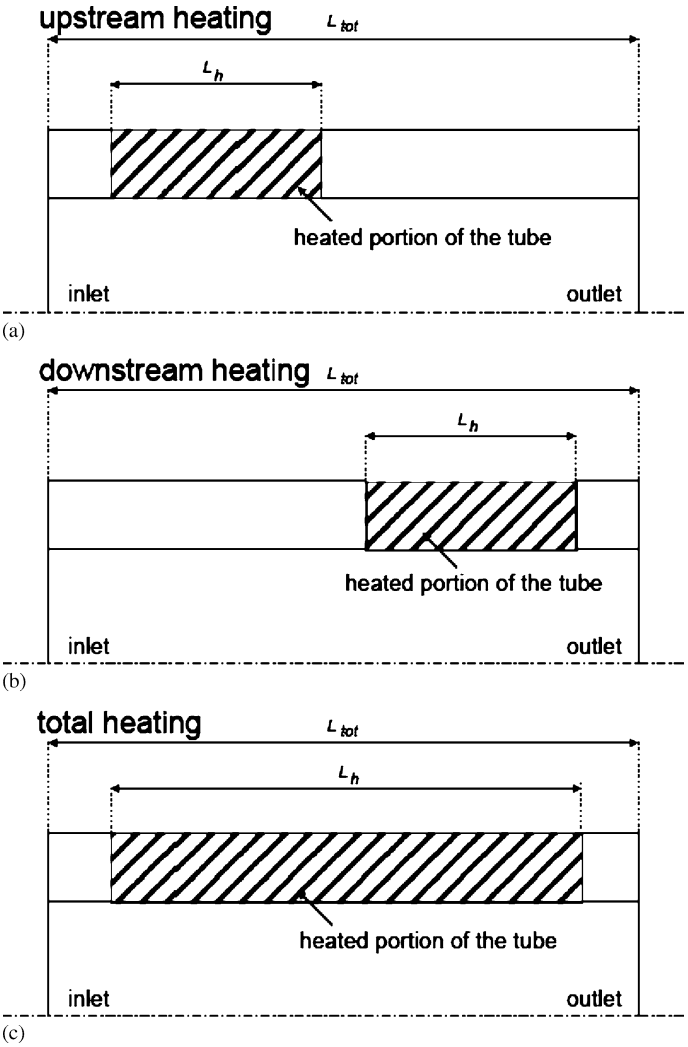

Fig. 4.1a–c Different heating cases in experiments and numerical modeling. Reprinted from Lelea (2005) with permission

Considering the available literature on the experimental research, one can conclude that there is a large scatter in the results on heat transfer. There is no convincing explanation of the difference between experimental and theoretical results for laminar flow, and between experimental and semi-empirical results for turbulent flow. On the one hand, several researchers argue that some new effects exist in micro-channels, e.g., Ho and Tai (1998), Tso and Mahulikar (1998, 1999, 2000), Gad-el-Hak (2003). On the other hand, the phenomenon can be related to the discrepancy between the actual conditions of a given experiment, and theoretical or numerical solution obtained in the frame of conventional theory (Herwig 2000; Herwig and Hausner 2003). The aim of the present chapter is to address this issue. The problem of heat transfer is considered here in the frame of a continuum model, corresponding to small Knudsen number. The data on heat transfer in circular, triangular, rectangular, and trapezoidal micro-channels with hydraulic diameters ranging from 10 to 2,000 μm are analyzed. The effects of geometry, axial heat flux due to thermal conduction through the working fluid and channel walls, and energy dissipation are also discussed. We focus on comparing experimental data, obtained by a number of investigators, to the conventional theory of heat transfer. The analysis includes a discussion of possible sources of unexpected effects reported in some experimental investigations.

In our analysis, we discuss experimental results of heat transfer obtained by previous investigators and related to incompressible fluid flow in micro-channels of different geometry. The basic characteristics of experimental conditions are given in Table 4.1. The studies considered herein were selected to reveal the physical basis of scale effect on convective heat transfer and are confined mainly to consideration of laminar flows that are important for comparison with conventional theory.

Table 4.1 Basic characteristics of micro-channels and experimental conditions

Cross-section	Micro-channel size			Working fluid	Walls		Re
	d_h [μm]	L [mm]	L/d_h		Material	Surface	
Circular	125.4–1,070	53–335	72–500	Distilled water, de-ionized water	Stainless steel	Smooth Rough	10–2,600
Rect-angular	133–2,000	25–325.125	13–433	De-min-eralized water, de-ionized water	Silicon, copper	Smooth Rough	40–9,000
Trapez-oidal and triangular	62.3–168.9	30	180–500	R-134a FC-84	Silicon	Smooth Rough	15–1,450

4.2 Experimental Investigations

4.2.1 Heat Transfer in Circular Tubes

Laminar flow

The schemes of the test sections used by some investigators are shown in Fig. 4.2. The geometrical parameters are presented in Tables 4.2 and 4.3.

Figure 4.2a shows the experimental set-up used by Lelea et al. (2004). The inner diameters of smooth micro-tubes were 125.4, 300, and 500 μm and the flow regime was laminar with Reynolds number Re = 95−774. The micro-tube was placed inside a vacuum chamber to eliminate heat loss to the ambient. It was heated by Joule heating with an electrical power supply. Distilled water was used and the measurements of heat transfer coefficient were performed under the thermal boundary condition of a constant heat flux on the wall. In the experimental set-up, there were two electrodes at both ends of the test tube. The insulated parts were included in the test section. Thus, for the heating length of $L_h = 250$, 95, and 53 mm the total length of the test section was $L = 600$, 123, and 70 mm, respectively. The experimental results have been compared both with theoretical predictions from the literature, and the results obtained by numerical modeling under the same thermal boundary conditions at the inlet and outlet of the tube. The experimental results confirm that the conventional theories are applicable for water flow through micro-channels, including the entrance effects (see Fig. 4.3a).

Table 4.2 Smooth circular micro-channels: experimental conditions

Author	Number of channels in the test section	Inner diameter d_{in} [μm]	Outer diameter d_{out} [μm]	Heating length L_h [mm]	Dimensionless length L_h/d_{in}	Reynolds number Re
Lelea et al. (2004)	1	500 300 125.4	700 500 300	250 95 53	500 317 424	95–774
Hetsroni et al. (2004)	1	1,070	1,500	335	313	10–450

Table 4.3 Rough circular micro-channels: experimental conditions

Author	Number of channels in the test section	Inner diameter d_{in} [μm]	Relative roughness k_s/d_{in}	Heating length L_h [mm]	Dimensionless length L_h/d_{in}	Reynolds number Re
Kandlikar et al. (2003)	1	1,067 620	0.00178–0.00281 0.00161–0.00355	76.5 67	72 108	500–2,600

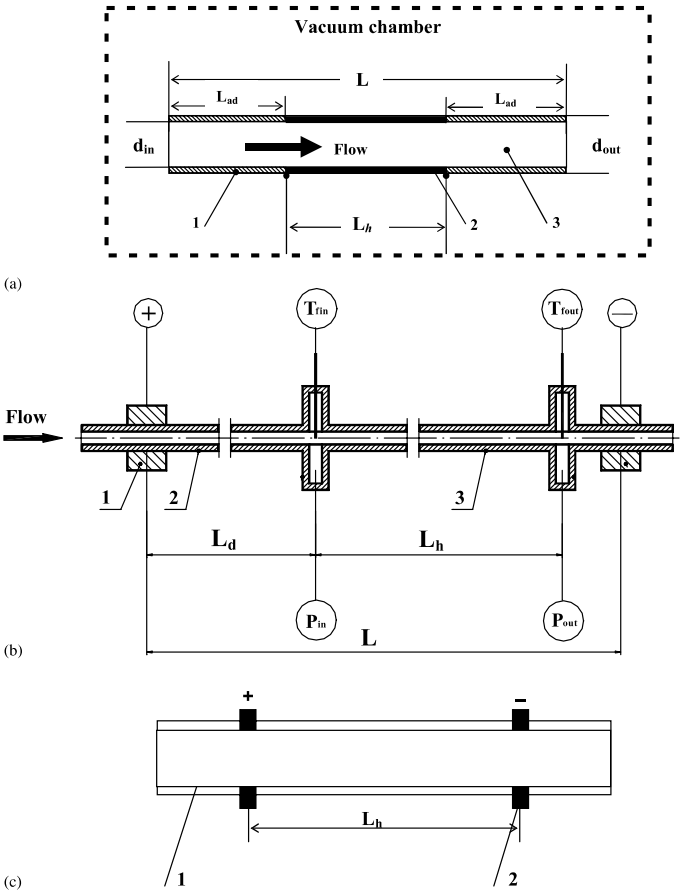

Fig. 4.2a–c Circular micro-channels. (**a**) $d_{\text{in}} = 125.4-500\,\mu\text{m}$. Test section used by Lelea et al. (2004) (schematic view): *1* adiabatic section, *2* heated section, *3* micro-channel. (**b**) $d_{\text{in}} = 1{,}070\,\mu\text{m}$. Test section used by Hetsroni et al. (2004): *1* electrical contact, *2* thermal developing section, *3* measurement section. (**c**) Test section of rough circular micro-channel used by Kandlikar et al. (2003) (schematic view). $d_{\text{in}} = 1{,}067\,\mu\text{m}$, $k_{\text{s}}/d_{\text{in}} = 0.00178-0.00281$; $d_{\text{in}} = 620\,\mu\text{m}$, $k_{\text{s}}/d_{\text{in}} = 0.00161-0.00355$: *1* steel tube, *2* electrical contact. Reprinted from Lelea et al. (2004), Hetsroni et al. (2004), and Kandlikar et al. (2003) with permission

The micro-channels utilized in engineering systems are frequently connected with inlet and outlet manifolds. In this case the thermal boundary condition at the inlet and outlet of the tube is not adiabatic. Heat transfer in a micro-tube under these conditions was studied by Hetsroni et al. (2004). They measured heat transfer to water flowing in a pipe of inner diameter 1.07 mm, outer diameter 1.5 mm, and 0.600 m in length, as shown in Fig. 4.2b. The pipe was divided into two sections. The development section of $L_{\text{d}} = 0.245$ m was used to obtain fully developed flow and thermal fields. The test section proper, of heating length $L_{\text{h}} = 0.335$ m, was used for collecting the experimental data.

DC current was supplied through the development and test sections for direct heating. The outer temperature on the heated wall was measured by means of an infrared radiometer. Experiments were carried out in the range of Re = 10−450. The average Nusselt number was calculated using the average temperature of the inner tube wall and mean temperature of the fluid at the inlet and outlet of the tube.

The dependence of the local Nusselt number on non-dimensional axial distance X^+ is shown in Fig. 4.3a. The dependence of the average Nusselt number on the Reynolds number is presented in Fig. 4.3b. The Nusselt number increased drastically with increasing Re at very low Reynolds numbers, $10 < \mathrm{Re} < 100$, but this increase became smaller for $100 < \mathrm{Re} < 450$. Such a behavior was attributed to the effect of axial heat conduction along the tube wall. Figure 4.3c shows the dependence of the relation N_a/N on the Peclet number Pe, where N_a is the power conducted axially in the tube wall, and N is total electrical power supplied to the tube. Comparison between the results presented in Fig. 4.3b and those presented in Fig. 4.3c allows one to conclude that the effect of thermal conduction in the solid wall leads to a decrease in the Nusselt number. This effect decreases with an increase in the

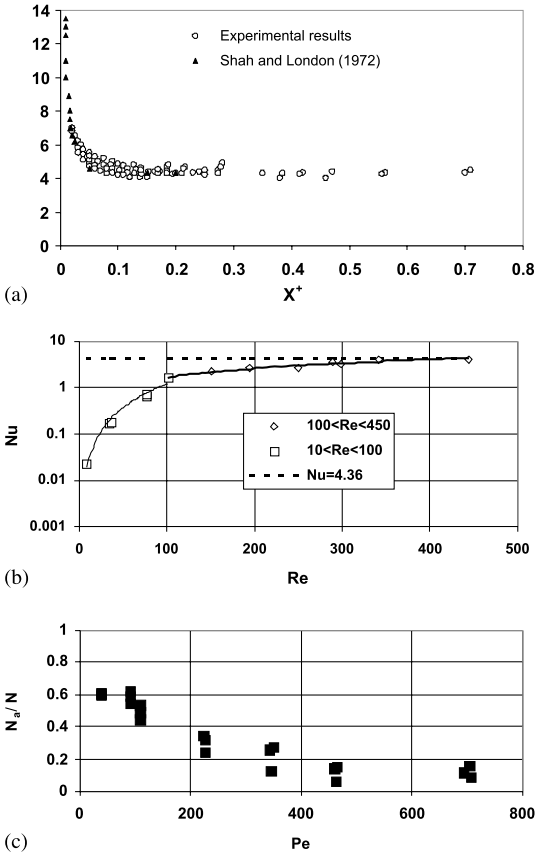

Fig. 4.3a–c Experimental results for smooth circular tubes. (**a**) Dependence of the Nusselt number on non-dimensional axial distance $d_{in} = 125.4$, 300 and 500 μm, Re = 95−774. Reprinted from Lelea et al. (2004) with permission. (**b**) $d_{in} =$ 1,070 μm. Dependence of average Nusselt number on Reynolds number. Reprinted from Hetsroni et al. (2004) with permission. (**c**) $d_{in} =$ 1,070 μm. Dependence of the relation of the power conducted axially through the heated wall to the power supplied to the heat section. Reprinted from Hetsroni et al. (2004) with permission

Reynolds number. It should be stressed that the heat transfer coefficient depends on the character of the wall temperature and the bulk fluid temperature variation along the heated tube wall. It is well known that under certain conditions the use of mean wall and fluid temperatures to calculate the heat transfer coefficient may lead to peculiar behavior of the Nusselt number (see Eckert and Weise 1941; Petukhov 1967; Kays and Crawford 1993). The experimental results of Hetsroni et al. (2004) showed that the use of the heat transfer model based on the assumption of constant heat flux, and linear variation of the bulk temperature of the fluid at low Reynolds number, yield an apparent growth of the Nusselt number with an increase in the Reynolds number, as well as underestimation of this number.

Turbulent flow

Adams et al. (1998) investigated turbulent, single-phase forced convection of water in circular micro-channels with diameters of 0.76 and 1.09 mm. The Nusselt numbers determined experimentally were higher than those predicted by traditional Nusselt number correlations such as the Gnielinski correlation (1976). The data suggest that the extent of enhancement (deviation) increases as the channel diameter decreases. Owhaib and Palm (2004) investigated the heat transfer characteristics

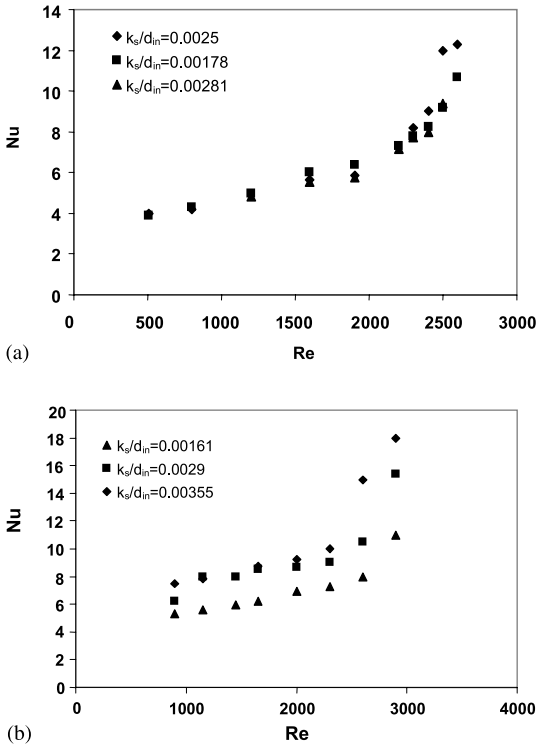

Fig. 4.4a,b Plots of local Nusselt number for different k_s/d_{in} ratios. (**a**) $d_{in} =$ 1,067 μm (**b**) $d_{in} = 620$ μm. Reprinted from Kandlikar et al. (2003) with permission

for single-phase forced convection of R-134 through single circular micro-channels. The test sections consisted of stainless steel tubes with 1.7, 1.2, and 0.8 mm inner diameters, and 325 mm in length. The results show good agreement between the classical correlations (Dittus-Boelter 1930; Petukhov et al. 1973; Gnielinski 1976) and the experimentally measured data in the turbulent region. Yang and Lin (2007), Lin and Yang (2007) measured the heat transfer coefficients for water flow through stainless steel micro-tubes with inner diameters ranging from 123 to 962 μm by the method of liquid crystal thermography. In the range of Re = 200−20,000, roughness surface of 1.16–1.48 μm the transfer correlations for laminar and turbulent flow can be well applied for predicting the fully developed heat transfer performances in micro-tubes. The transition occurs at Reynolds numbers from 2,300 to 3,000. This is also the same range as that for convectional tubes. On the contrary, correlations suggested for micro-channels (Wu and Little 1984; Choi et al. 1991; Adams et al. 1998) do not agree with this test. Kandlikar et al. (2003) studied experimentally the effect of surface roughness on heat transfer in circular tubes 1.067 and 0.62 mm in diameter. Brief details of these experiments are given in Fig. 4.2c and Table 4.3. The results are presented in Fig. 4.4a,b. They concluded that tubes above $d_{in} = 1.067$ mm with relative roughness k_s/d_{in} about 0.003 may be considered as smooth tubes. However, for small diameter tubes ($d_{in} < 0.62$ mm), the same relative roughness increases the heat transfer.

4.2.2 Heat Transfer in Rectangular, Trapezoidal and Triangular Ducts

The schemes of the test sections reported in the literature are shown in Fig. 4.5. The geometrical parameters are presented in Tables 4.4 and 4.5. Peng and Peterson (1996) investigated experimentally the single-phase forced convective heat transfer

Table 4.4 Rectangular micro-channels

Author	Number of channels in the test section	Heating length L_h [mm]	Hydraulic diameter d_h [μm]	Dimensionless length L_h/d_h	Reynolds number Re
Peng and Peterson (1996)	Not reported	45	133–367	123–338	90–9,000
Harms et al. (1999)	1 68	25	1,923 404	13 62	173–12,900
Qu and Mudawar (2002b)	21	44.764	348	129	139–1,672
Warrier et al. (2002)	5	325.125	750	433.5	557–1,552
Gao et al. (2002)	1	62	200–2,000	31–310	40–8,000
Lee et al. (2005)	10	25.4	318–903	28–80	300–3,500

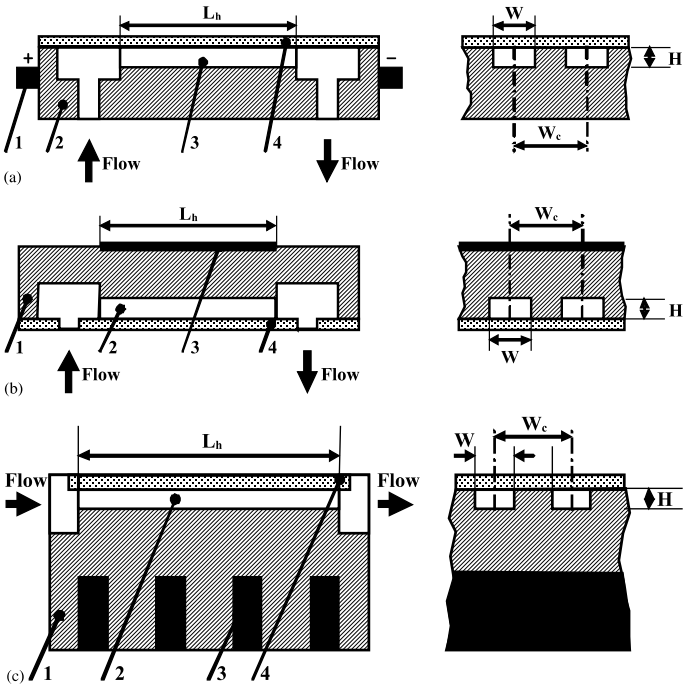

Fig. 4.5a–c Rectangular micro-channels. (**a**) $d_h = 133-367$ µm. Test section used by Peng and Peterson (1996) (schematic view): *1* electrical contact, *2* heated stainless steel block, *3* micro-channel, *4* cover plate. (**b**) $d_h = 404-1{,}923$ µm. Test section used by Harms et al. (1999) (schematic view): *1* silicon wafer, *2* micro-channel, *3* heater, *4* cover plate. (**c**) $d_h = 348$ µm. Test section used by Qu and Mudawar (2002a) (schematic view): *1* copper block, *2* micro-channel, *3* heater, *4* cover plate. Reprinted from Peng and Peterson (1996), Harms et al. (1999), Warrier et al. (2002), Qu and Mudawar (2002a), Gao et al. (2002), and Lee et al. (2005) with permission

Table 4.5 Trapezoidal and triangular micro-channels

Author	Number of channels in the test section	Length L [mm]	Hydraulic diameter d_h [µm]	Dimension-less length L/d_h	Relative roughness k_s/d_h	Reynolds number Re
Qu et al. (2000)	5	30	62.3 168.9	482 178	1.12×10^{-2} 1.75×10^{-2}	100–1,450
Wu and Cheng (2003)	13			195.34–453.79	3.26×10^{-5}–1.09×10^{2}	15–1,500
Tiselj et al. (2004)	17	10	160	63		3.2–84

of water in micro-channel structures with small rectangular channels having a hydraulic diameter of 0.133–0.367 mm and the distinct geometric configuration shown in Fig. 4.5a. The heat flux of the micro-channel structure was based on the micro-

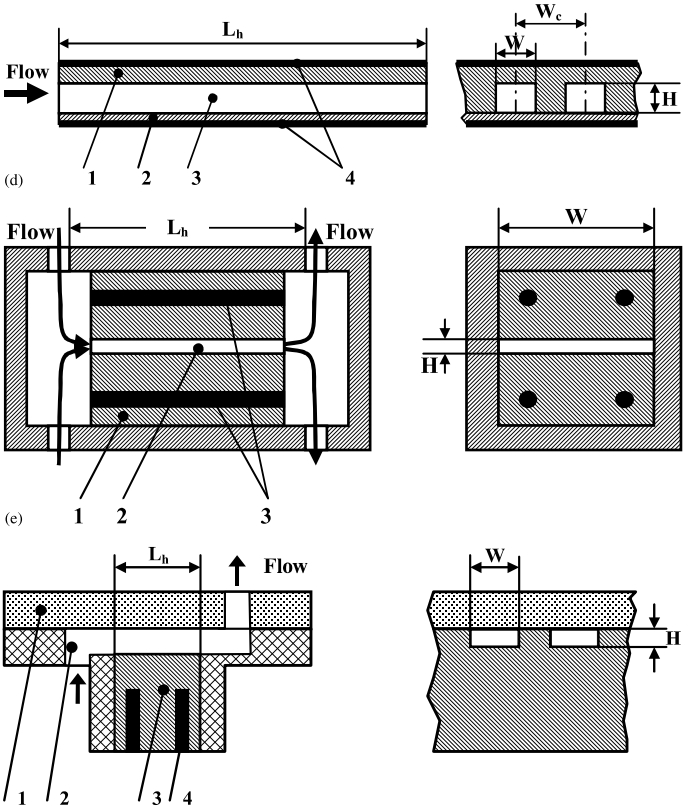

Fig. 4.5d–f Rectangular micro-channels. (**d**) $d_h = 750\,\mu m$. Test section used by Warrier et al. (2002) (schematic view): *1* upper aluminum plate, *2* down aluminum plate, *3* micro-channel, *4* heater. (**e**) $d_h = 200-2{,}000\,\mu m$. Test section used by Gao et al. (2002) (schematic view): *1* brass block, *2* micro-channel, *3* heater. (**f**) Thermally developing flow in rectangular micro-channel (Lee et al. 2005) (schematic view): *1* cover plate, *2* micro-channel, *3* copper block, *4* heater. Reprinted from Peng and Peterson (1996), Harms et al. (1999), Warrier et al. (2002), Qu and Mudawar (2002a), Gao et al. (2002), and Lee et al. (2005) with permission

channel plate area. The heat transfer coefficient was evaluated using the log-mean temperature difference. Thus, the heat transfer coefficient corresponds to some integral value of heat flux. The dependence of the heat transfer coefficient on the flow and geometric parameters was presented.

Harms et al. (1999) obtained experimental results for single-phase forced convection in deep rectangular micro-channels (Fig. 4.5b). Two configurations were tested, a single-channel system and a multiple-channel system. All tests were performed with de-ionized water, and Reynolds number ranging from 173 to 12,900. For the single channel design, the experimental Nusselt number was higher than theoretically predicted for heat transfer in laminar flow. For example, at $Re = 1{,}383$

the Nusselt number was Nu = 40.9. Harms et al. (1999) concluded that this enhancement may be due to the effect of the inlet bend. The results for the multiple channel design in the range Re = 173−1,188 showed an increase in Nusselt number with increasing Re. For example, at Re = 173 the Nusselt number was equal to 2.65, and at Re = 1,188 the Nusselt number was 8.41. This deviation from theoretical prediction was attributed to flow bypass in the manifold. The authors believe that in systems with a small heater area compared to the projected channel area, three-dimensional conduction occurs. However, for multiple channel design three-dimensional conduction also occurs when the heater area covers the entire projected channel area.

Qu and Mudawar (2002b) studied both experimentally and numerically heat transfer characteristics of a single-phase micro-channel heat sink. The heat sink was made from oxide-free copper and fitted with a polycarbonate plastic cover plate (Fig. 4.5c). The heat sink consisted of an array of rectangular micro-channels 231 μm wide and 713 μm deep (Table 4.4). The Reynolds number ranged from 139 to 1,672. The three-dimensional heat transfer characteristics of the heat sink were analyzed numerically by solving the conjugate heat transfer problem. The measured temperature distributions showed good agreement with the corresponding numerical predictions (Fig. 4.6a). These findings demonstrate that conventional Navier–Stokes and energy equations can adequately predict the fluid flow and heat transfer characteristics of micro-channel heat sinks.

Warrier et al. (2002) conducted experiments of forced convection in small rectangular channels using FC-84 as the test fluid. The test section consisted of five parallel channels with hydraulic diameter $d_h = 0.75$ mm and length-to-diameter ratio $L_h/d_h = 433.5$ (Fig. 4.5d and Table 4.4). The experiments were performed with uniform heat fluxes applied to the top and bottom surfaces. The wall heat flux was calculated using the total surface area of the flow channels. Variation of single-phase Nusselt number with dimensionless axial distance is shown in Fig. 4.6b. The numerical results presented by Kays and Crawford (1993) are also shown in Fig. 4.6b. The measured values agree quite well with the numerical results.

The study of Gao et al. (2002) is devoted to investigations of the flow and associated heat transfer in micro-channels of large-span rectangular cross-section and adjustable height in the range of $H = 0.1-1$ mm (Fig. 4.5e and Table 4.4). The fluid used was de-mineralized water. The active channel walls were two plane brass blocks of heating length $L_h = 62$ mm, which were separated by a foil with a hollowed out central part of width $W = 25$ mm. The thickness of this foil fixed the channel height, H. A set of foils allowed variations of the hydraulic diameter d_h from 200 to 2,000 μm. A typical temperature distribution along the channel for the case of a very narrow micro-channel ($d_h = 200$ μm) is shown in Fig. 4.6c, where TC1 through TC5 denote thermocouples. The local Nusselt number Nu_x expressed as a function of $X^+ = x/(d_h Pe)$, was compared with the theoretical solution of Shah and London (1978). For $H = 1$ mm the results demonstrate good agreement with the theoretical solution. However, for $H = 0.1$ mm, the plot $Nu(X^+)$ shows departure from the theoretical heat transfer law, as the Nusselt number is smaller than the conventional value for large-scale channels. This trend is in agreement with results

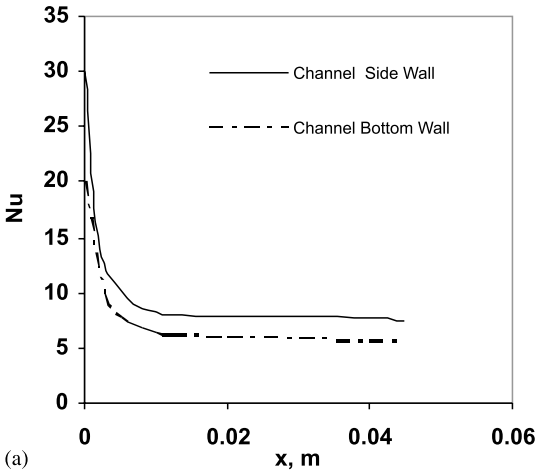

(a)

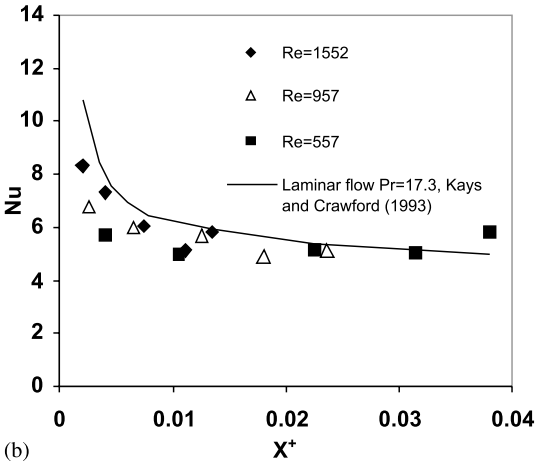

(b)

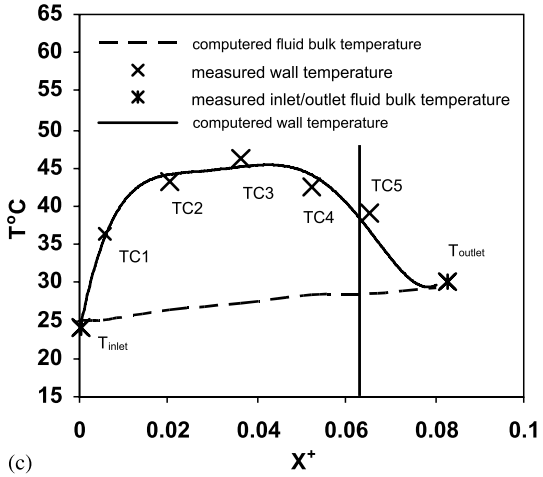

(c)

Fig. 4.6a–c Rectangular micro-channels. Calculation and experimental data for (**a**) $d_h = 348\ \mu m$. Numerical predictions of average Nusselt number, Re = 864 (Qu and Mudawar 2002). (**b**) $d_h = 750\ \mu m$. Variation of Nusselt number with axial distance (Warrier et al. 2002). (**c**) $d_h = 200\ \mu m$, Re = 1,780. Temperature distribution along the channel (Gao et al. 2002). Reprinted from Qu and Mudawar (2002), Warrier et al. (2002), Goa et al. (2002), and Lee et al. (2005) with permission

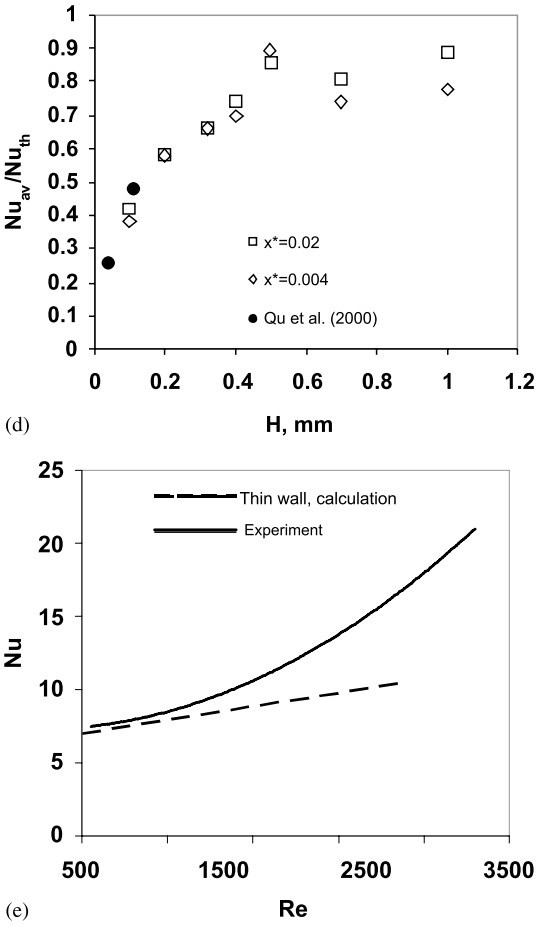

Fig. 4.6d,e Rectangular micro-channels. (**d**) d_h = 200−2,000 μm. Effect of channel size on Nusselt number (Gao et al. 2002). (**e**) Comparison of the average Nusselt number obtained from numerical analyses for the 194 μm wide micro-channels (Lee et al. 2005). Reprinted from Qu and Mudawar (2002), Warrier et al. (2002), Goa et al. (2002), and Lee et al. (2005) with permission

reported by Qu et al. (2000). Figure 4.6d shows the dependence of Nu_{av}/Nu_{th} as a function of the channel height, where Nu_{th} is the theoretical value of the Nusselt number for the same value of X^+. The significant reduction in the Nusselt number cannot be explained by roughness effects. The modification of heat transfer laws by electrokinetic effects also should be discarded, due to the large difference of scales between the channel height and the double-diffusive layer thickness.

An experimental investigation was conducted by Lee et al. (2005) to explore the validity of classical correlations based on conventional sized channels for predicting the thermal behavior in single-phase flow through rectangular micro-channels. The micro-channels ranged in width from 194 to 534 μm, with the channel depth being nominally five times the width in each case (Fig. 4.5f and Table 4.4). Each test piece was made of copper and contained ten micro-channels in parallel. The experiments were conducted with de-ionized water, with Reynolds number ranging from approximately 300 to 3,500. The tests were carried out either at the hydrodynamically

developed but thermally developing (TD) regime or a simultaneously developing (SD) regime. The average heat transfer coefficient was determined by using the area available for convection of channels, average temperature of the channel wall and mean fluid temperature at the inlet and outlet of the micro-channels. In Fig. 4.6e the numerical calculations that did not include the conduction in the substrate (thin wall) are compared with the experimental results.

Qu et al. (2000) carried out experiments on heat transfer for water flow at $100 < \mathrm{Re} < 1{,}450$ in trapezoidal silicon micro-channels, with the hydraulic diameter ranging from 62.3 to 168.9 μm. The dimensions are presented in Table 4.5. A numerical analysis was also carried out by solving a conjugate heat transfer problem involving simultaneous determination of the temperature field in both the solid and fluid regions. It was found that the experimentally determined Nusselt number in micro-channels is lower than that predicted by numerical analysis. A roughness-viscosity model was applied to interpret the experimental results.

Wu and Cheng (2003) investigated laminar convective heat transfer of water in a single trapezoidal silicon micro-channel. They used a set of 13 micro-channels having different dimensions and different relative roughness. The geometrical parameters of micro-channels are presented in Table 4.5. A silicon chip was anodically bonded with a thin Pyrex glass plate from the top. Figure 4.7a shows the effect of relative surface roughness, a, on the Nusselt number, where W_t and W_b are the width (μm) of the channels top and bottom, respectively, and H is the height of the channel (in microns). One can see that at the same Reynolds numbers the Nusselt number increases with increasing relative surface roughness. The laminar convective heat transfer showed two different characteristics at low and high Reynolds number ranges. Figure 4.7b shows the effect of geometric parameters on the Nusselt number, in the range of relative surface roughness $a = 3.62 \times 10^{-5} - 9.85 \times 10^{-5}$. From Fig. 4.7b it can be observed that for very low Reynolds number flow, $\mathrm{Re} = 0-100$, the Nusselt number increased acutely with the increase in the Reynolds number. However, the increase in the Nusselt number when $\mathrm{Re} > 100$ is gentle with an increase in the Reynolds number.

4.2.3 Heat Transfer in Surfactant Solutions Flowing in a Micro-Channel

The dependence of the average heat transfer coefficient on the bulk fluid velocity is plotted in Fig. 4.8. These data are related to laminar flow of Habon G aqueous solutions of $C = 530$ ppm (H530) and $C = 1{,}200$ ppm (H1200) in a micro-channel with the inner diameter of 1.07 mm (Hetsroni et al. 2004). The figure shows that the heat transfer coefficient in surfactant solutions is higher than in laminar pipe water flow. Figure 4.9 shows relative enhancement in heat transfer coefficient $\mathrm{DR}(h) = (1 - h_\mathrm{sur}/h_\mathrm{wat})$ versus fluid bulk velocity, where h_sur and h_wat are the heat transfer coefficients in the tube at the same bulk velocity of surfactant solution, Habon G and water, respectively. Note that data for $C = 530$ ppm and $C = 1{,}060$ ppm

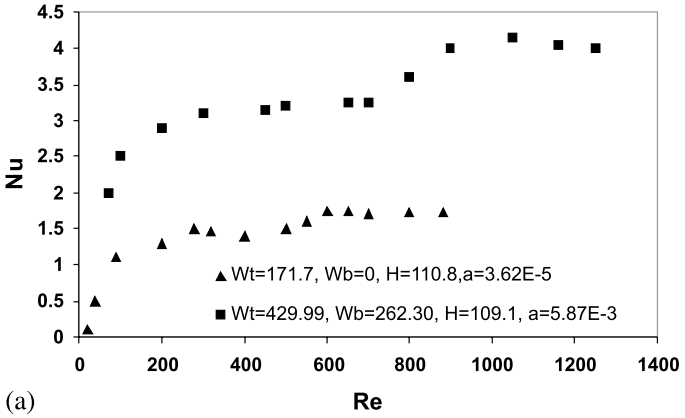

Fig. 4.7a,b Trapezoidal micro-channels. (**a**) Effect of surface roughness on Nusselt number (Wu and Cheng 2003). (**b**) Effect of geometric parameters on Nusselt number (Wu and Cheng 2003). Reprinted from Wu and Cheng (2003) with permission

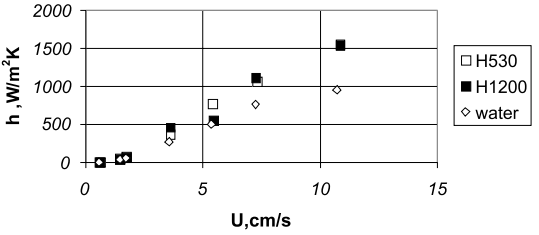

Fig. 4.8 Average heat transfer coefficient dependence on flow velocity. Reprinted from Hetsroni et al. (2004) with permission

are expressed as the same symbols. The negative values of DR(h) correspond to an increase in the heat transfer coefficient. It can be seen from Fig. 4.9 that the increase in the heat transfer coefficient does not depend on the solution bulk velocity. With the addition of surfactant macromolecules to water, the viscosity and pressure drop in laminar pipe flows increase. It is thus quite unexpected to find that for heat transfer the opposite can sometimes take place. Kostic (1994) observed that some drag-reducing solutions augmented the heat transfer in laminar flow in a non-circular

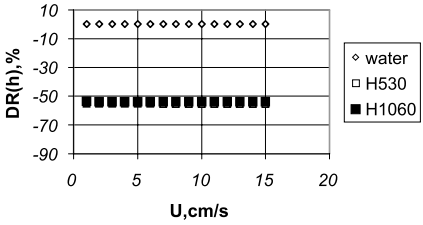

Fig. 4.9 Relative heat transfer coefficient on liquid velocity. Reprinted from Hetsroni et al. (2004) with permission

duct. They suggested that the fluid elasticity may lead to secondary flows, which are responsible for the increase in the heat transfer. The secondary flows increase the pressure drops in both adiabatic and diabatic flows. However, in diabatic flow the total pressure drop (due to friction and due to secondary flows) may be smaller compared to that in the adiabatic flow. In this case the common effect includes also some decrease in the fluid viscosity with an increase in the temperature of the surfactant solution. On the other hand, it may be assumed that macromolecules of surfactant change the flow structure in the near-wall region. It also may be responsible for the increase in pressure drop and heat transfer.

The average Nusselt number, Nu, is presented in Fig. 4.10a,b versus the shear Reynolds number, Re_{sh}. This dependence is qualitatively similar to water behavior for all surfactant solutions used. At a given value of Reynolds number, Re_{sh}, the Nusselt number, Nu, increases with an increase in the shear viscosity. As discussed in Chap. 3, the use of shear viscosity for the determination of drag reduction is not a good choice. The heat transfer results also illustrate the need for a more appropriate physical parameter. In particular, Fig. 4.10a shows different behavior of the Nusselt number for water and surfactants. Figure 4.10b shows the dependence of the Nusselt number on the Peclet number. The Nusselt numbers of all solutions are in agreement with heat transfer enhancement presented in Fig. 4.8. The data in Fig. 4.10b show

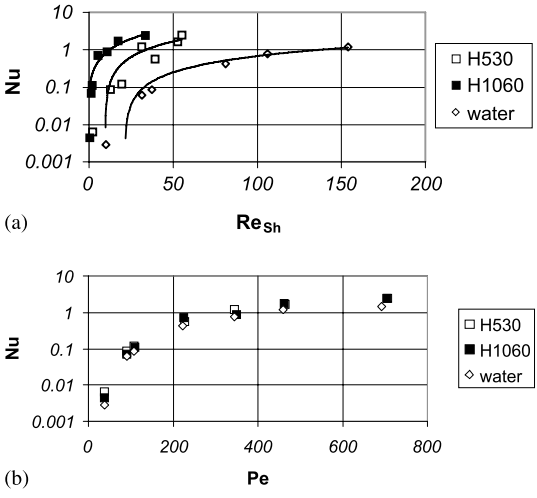

Fig. 4.10a,b The dependence of the Nusselt number on the Reynolds and Peclet numbers. (**a**) Dependence of the average Nusselt number on the solution Reynolds number. (**b**) Dependence of the Nusselt number on the Peclet number. Reprinted from Hetsroni et al. (2004) with permission

that the use of the Peclet number may be considered for description of experimental data of laminar pipe flow of certain non-Newtonian fluids.

4.3 Effect of Viscous Energy Dissipation

Under some conditions, the heat released due to viscous dissipation leads to a drastic change of flow and temperature field: in particular, it leads to flow instability, transition to turbulence, oscillatory motions, etc. (Gruntfest et al. 1964; Bastanjian et al. 1965; Zel'dovich et al. 1985; Hetsroni et al. 2005). This problem was also discussed by Tso and Mahulikar (1998, 1999, 2000). To reveal the effect of viscous dissipation, the experimental data by Wang and Peng (1994) and Tso and Mahulikar (2000) were used. Experiments were performed using water flow in microchannels. The experimental data in the laminar flow regime were found to correlate well with the Brinkman number. As a result, a semi-empirical equation for the Nusselt number was suggested and the dependence of $\mathrm{Nu}/\mathrm{Re}^{0.62}\,\mathrm{Pr}^{0.33}$ on the Brinkman number was demonstrated. The Brinkman number, $\mathrm{Br} = \mu U^2/k\Delta T$, is the ratio of the heat production due to viscous forces, to heat transferred from the wall to the fluid. However, most of the data used for that correlation were obtained under conditions in which the Reynolds number and the Prandtl number also varied, so that it was difficult to separate the effect of the Brinkman number from the effects of the Reynolds and Prandtl numbers. For instance, at $0.4559\times10^{-5} \le \mathrm{Br} \le 2.8333\times10^{-5}$ the Reynolds and Prandtl numbers varied as $80 \le \mathrm{Re} \le 107$, and $4.80 \le \mathrm{Pr} \le 6.71$ (Tso and Mahulikar 1998). To estimate the real effect of viscous dissipation on heat transfer it is necessary to determine the dependence of the Nusselt number on the Brinkman number at fixed values of the Reynolds and the Prandtl numbers. This is done for the data reported by Tso and Mahulikar (1998) as shown in Table 4.6. One can see that the effect of the Brinkman number on the Nusselt number is negligible. The same conclusion may be derived also from experiments performed by Tso and Mahulikar (2000). According to their measurements (Table 4.7) variation of the Brinkman number from 1.1195×10^{-8} to 2.3048×10^{-8} did not affect the Nusselt number, when the Reynolds and the Prandtl numbers did not change significantly. It should be stressed that the effect of viscous dissipation on heat transfer in microchannels at extremely small values of the Brinkman number, $\mathrm{Br} \sim 10^{-8}-10^{-5}$, is

Table 4.6 Experimental data in the laminar regime presented by Tso and Mahulikar (1998) at approximately fixed values of the Reynolds and the Prandtl numbers

$\mathrm{Br}\times10^5$	Re	Pr	Nu
0.4559	107	4.80	0.35
1.4541	124	4.82	0.37
2.8333	80	6.71	0.46
4.4115	93	6.62	0.49

Table 4.7 Experimental data in the laminar regime obtained by Tso and Mahulikar (2000) at approximately fixed values of the Reynolds and the Prandtl numbers

$\mathrm{Br} \times 10^8$	Re	Pr	Nu
1.1195	17.5	3.50	0.3031
2.3048	22.4	3.82	0.3068

not realistic from the physical point of view. At small Br the contribution of the heat released due to viscous forces is negligible, consequently the effect on the heat transfer is also negligible. It should also be noted that evaluation of the role of the Brinkman number performed by Tso and Mahulikar (1998, 1999, 2000) was based on the experiments that were carried out under some specific conditions (the heat transfer characteristics were found to be affected by the channel geometry, axial heat conduction in the channels walls, liquid velocity and temperature, etc.). Some aspects of this problem were discussed by Herwig and Hausner (2003) and Gad-el-Hak (2003).

The effect of viscous heating was investigated by Tunc and Bayazitoglu (2001) when the fluid was heated ($T_{\mathrm{in}} < T_{\mathrm{w}}$) or cooled ($T_{\mathrm{in}} > T_{\mathrm{w}}$). In the range of $0 < \mathrm{Kn} < 0.12$ the Nusselt number decreased as the Knudsen number increased. The viscous dissipation significantly affected heat transfer. Tunc and Bayazitoglu (2001) showed that the decrease was greater when viscous dissipation occurred. The effect of viscous dissipation on the temperature field was investigated by Koo and Kleinstreuer (2004) for three working fluids: water, methanol and isopropanol. Channel size, the Reynolds number and the Prandtl number are the key factors, which determine the impact of viscous dissipation. Viscous dissipation effects may be very important for fluids with low specific heats and high viscosities, even in relatively low Reynolds number flows. For water the relative magnitude of the ratio, A_{d}, of convective heat transfer to dissipation term is given in Table 4.8.

Experimental and numerical analyses were performed on the heat transfer characteristics of water flowing through triangular silicon micro-channels with hydraulic diameter of 160 μm in the range of Reynolds number $\mathrm{Re} = 3.2-84$ (Tiselj et al. 2004). It was shown that dissipation effects can be neglected and the heat transfer may be described by conventional Navier–Stokes and energy equations as a common basis. Experiments carried out by Hetsroni et al. (2004) in a pipe of inner diameter of 1.07 mm also did not show effect of the Brinkman number on the Nusselt number in the range $\mathrm{Re} = 10-100$.

Table 4.8 Ratio A_{d} of convective heat transfer to dissipation term in tubes

Tube radius r_0 [m]	$\mathrm{Re} = 20A_{\mathrm{d}}$	$\mathrm{Re} = 200A_{\mathrm{d}}$	$\mathrm{Re} = 2{,}000A_{\mathrm{d}}$
10^{-3}	3.45×10^4	3.45×10^3	3.45×10^2
10^{-4}	3.45×10^2	3.45×10^1	3.45×10^0
10^{-5}	3.45×10^0	3.45×10^{-1}	3.45×10^{-2}

Hetsroni et al. (2005) evaluated the effect of inlet temperature, channel size and fluid properties on energy dissipation in the flow of a viscous fluid. For fully developed laminar flow in circular micro-channels, they obtained an equation for the adiabatic increase of the fluid temperature due to viscous dissipation:

$$\frac{\Delta T}{T_{\text{in}}} = 2\frac{v^2}{r_0^2}\left(\frac{L}{r_0}\right)\frac{\text{Re}}{c_{\text{p}}T_{\text{in}}}. \tag{4.1}$$

For an incompressible fluid, the density variation with temperature is negligible compared to the viscosity variation. Hence, the viscosity variation is a function of temperature only and can be a cause of radical transformation of flow and transition from stable flow to the oscillatory regime. The critical Reynolds number also depends significantly on the specific heat, Prandtl number and micro-channel radius. For flow of high-viscosity fluids in micro-channels of $r_0 < 10^{-5}$ m the critical Reynolds number is less than 2,300. In this case the oscillatory regime occurs at values of Re $<$ 2,300.

We can estimate the values of the Brinkman number, at which the viscous dissipation becomes important. Assuming that the physical properties of the fluid are constant, the energy equation for fully developed flow in a circular tube at $T_{\text{w}} = \text{const.}$ is:

$$\rho u c_{\text{p}}\frac{\partial T}{\partial x} = \frac{1}{r}\frac{\partial}{\partial r}\left(kr\frac{\partial T}{\partial r}\right) + \mu\left(\frac{\partial u}{\partial r}\right)^2 \tag{4.2}$$

where ρ, μ and k are the density, dynamic viscosity and thermal conductivity, respectively, c_{p} is the specific heat, and u is the actual streamwise velocity.

The actual velocity, u, may be expressed as:

$$u = 2U(1 - R^2) \tag{4.3}$$

where $U = \frac{1}{r_0^2}\int_0^{r_0} ur\,\text{d}r$ is the average velocity, and $R = \frac{r}{r_0}$, r_0 is the micro-channel radius.

From Eqs. (4.2) and (4.3) one can obtain:

$$\frac{2\int\limits_0^{r_0}\frac{\partial}{\partial x}\left\{\rho u c_{\text{p}}(T - T_{\text{w}})\right\}r\,\text{d}r}{k(\overline{T} - T_{\text{w}})} = -\text{Nu} \pm 8\,\text{Br} \tag{4.4}$$

where $\overline{T}$ is the average fluid temperature, T_{w} is the wall temperature, $\text{Nu} = -\left(k\left(\partial T/\partial r\right)_{r=r_0} d\right)/\left(k(\overline{T} - T_{\text{w}})\right)$ is the Nusselt number, and Br is the Brinkman number. The minus or plus sign in front of the last term in Eq. (4.4) corresponds to cooling of fluid when $\overline{T}_0 > T_{\text{w}}$ or its heating when $\overline{T}_0 < T_{\text{w}}$, respectively, where $\overline{T}_0$ is the average fluid temperature at the inlet of the micro-channel.

A detailed study of the influence of viscous heating on the temperature field in micro-channels of different geometries (rectangular, trapezoidal, double-trapezoidal) has been performed by Morini (2005). The momentum and energy conservation equations for flow of an incompressible Newtonian fluid were used to estimate

the effect of viscous dissipation on bulk temperature. For steady two-dimensional fully developed laminar flow with constant physical properties the following relation for longitudinal gradient of the bulk temperature was derived

$$\frac{\mathrm{d}T_b}{\mathrm{d}x} = \left\{ 4\frac{\mathrm{Ec}}{\mathrm{Re}}(\lambda \mathrm{Re}) \right\} \frac{\Delta T}{d_\mathrm{h}} \tag{4.5}$$

where $T_b = \frac{1}{A}\int_A u(y,z)T(x,y,z)\,\mathrm{d}A$ is the bulk temperature, A is the cross-section area, $u(y,z)$ and $T(x,y,z)$ are the longitudinal components of velocity and temperature, respectively, $\mathrm{Re} = U d_\mathrm{h}/\nu$ and $\mathrm{Ec} = U^2/\left(2c_\mathrm{p}\Delta T\right)$ are the Reynolds and Eckert numbers, λ is the friction factor, ΔT is the temperature difference, x,y,z are the Cartesian coordinates, and x is directed along the micro-channel axis.

The effect of viscous dissipation on temperature change along the micro-channel axis is illustrated in Fig. 4.11, where the dependences $\mathrm{d}T_b/\mathrm{d}x$ on d_h that correspond to water and isopropanol flows are presented. One can see that under the conditions corresponding to the Judy et al. (2002) experiments ($d_\mathrm{h} = 74.1\,\mu\mathrm{m}$, $L = 114\,\mathrm{mm}$, $L/d = 1{,}543$), the rise of bulk temperature due to viscous dissipation is small enough. So, at $d_\mathrm{h} \geq 100\,\mu\mathrm{m}$ the temperature gradient is $\mathrm{d}T_b/\mathrm{d}x \leq 1\,\mathrm{K/m}$. In this case, the difference between outlet and inlet temperature is about 0.1 K. Under conditions that are typical for micro-channels of electronic devices ($L/d_\mathrm{h} \sim 10^2$) this difference is about 0.01 K. The rise of temperature due to viscous dissipation is small enough even at water flow in micro-channels with $d_\mathrm{h} \sim 20\,\mu\mathrm{m}$. Thus, for micro-channels with $d_\mathrm{h} = 20\,\mu\mathrm{m}$ and $L/d_\mathrm{h} = 10^2$, we have $T_\mathrm{out} - T_\mathrm{in} \approx 0.8\,\mathrm{K}$.

To estimate the value of the term on the left-hand side of Eq. (4.4), we use an approximate expression for the local and average fluid temperature in the tube. We use

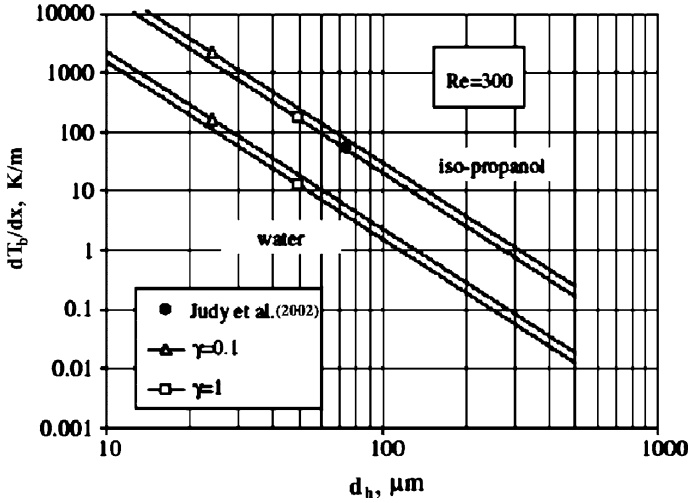

Fig. 4.11 Temperature gradients due to viscous dissipation at Re = 300. Flow in rectangular ($\gamma = 0.1$), and square ($\gamma = 1$) micro-channel. Reprinted from Morini (2005) with permission

as the initial guess the expressions for $T(x,r)$ and $\overline{T}(x)$ that correspond to negligible viscous dissipation. For $T_w = \text{const.}$ they are:

$$T - T_w = (T_0 - T_w) \sum_{n=0}^{\infty} A_n \varphi_n(R) \exp\left(-2\varepsilon_n^2 \frac{1}{\text{Pe}} \frac{x}{d}\right) \tag{4.6}$$

$$\overline{T} - T_w = 8(\overline{T}_0 - T_w) \sum_{n=1}^{\infty} \frac{B_n}{\varepsilon_n^2} \exp\left(-2\varepsilon_n^2 \frac{1}{\text{Pe}} \frac{x}{d}\right) \tag{4.7}$$

where $\text{Pe} = Ud/\alpha$ is the Peclet number, α is the thermal diffusivity, A_n and B_n are constants, ε_n and $\varphi_n(R)$ are the corresponding eigen functions (Petukhov 1967).

For large values of dimensionless axial distance, $X^+ = x/(\text{Pe}\, d)$ the following relations were obtained from Eqs. (4.4), (4.6), and (4.7):

$$T - T_w = (T_0 - T_w) A_0 \varphi_0(R) \exp\left(-2\varepsilon_0^2 \frac{1}{\text{Pe}} \frac{x}{d}\right) \tag{4.8}$$

$$\overline{T} - T_w = 8(\overline{T}_0 - T_w) \frac{B_0}{\varepsilon_0^2} \exp\left(-2\varepsilon_0^2 \frac{1}{\text{Pe}} \frac{x}{d}\right) \tag{4.9}$$

and:

$$-2 \frac{\frac{\text{d}}{\text{d}x} \int_0^{r_0} \rho u c_p T r \,\text{d}r}{k(\overline{T} - T_w)} = \frac{1}{4} \varepsilon_0^4 \frac{A_0}{B_0} \int_0^1 (1 - R^2) \varphi_0(R) R \,\text{d}R. \tag{4.10}$$

Substitution of the values of ε_0, A_0, B_0, as well as the expression for $\varphi_0(R)$ in the right hand side of Eq. (4.10) gives:

$$\frac{1}{4} \varepsilon_0^4 \frac{A_0}{B_0} \int_0^1 (1 - R^2) \varphi_0(R) R \,\text{d}R = 3.64 = \text{Nu}_0 \tag{4.11}$$

where Nu_0 is the Nusselt number that corresponds to negligible viscous dissipation.

Equation (4.4) is rewritten as:

$$\text{Nu} = \text{Nu}_0 \pm 8\,\text{Br} \tag{4.12}$$

where the plus and minus signs correspond to the cooling $\overline{T}_0 > T_w$ or heating $\overline{T}_0 < T_w$ regimes, respectively.

Equation (4.12) indicates the effect of viscous dissipation on heat transfer in micro-channels. In the case when the inlet fluid temperature, $\overline{T}_0$, exceeds the wall temperature, viscous dissipation leads to an increase in the Nusselt number. In contrast, when $\overline{T}_0 < T_w$, viscous dissipation leads to a decrease in the temperature gradient on the wall. Equation (4.12) corresponds to a relatively small amount of heat released due to viscous dissipation. Taking this into account, we estimate the lower boundary of the Brinkman number at which the effect of viscous dissipation may be observed experimentally. Assuming that $(\text{Nu} - \text{Nu}_0)/\text{Nu}_0 \geq 10^{-2}$ the follow-

ing evaluation of the Brinkman number was obtained: $\mathrm{Br} \geq 5 \times 10^{-3}$. This estimation shows that the conclusions of Tso and Mahulicar (1998, 1999, 2000) cannot be derived from experiments performed at extremely low Brinkman numbers of $\mathrm{Br} \sim 10^{8}-10^{5}$.

It should be noted that for some fluids, viscous dissipation can affect the development length in tubes at this physical scale, particularly at high average fluid velocities. The influence of viscous dissipation was explored by Judy et al. (2002). Viscous heating has the effect of increasing the temperature of the flowing fluid along the tube axis, yielding continuously varying thermophysical properties. The Nahme number is used by Judy et al. (2002) to estimate the importance of viscous dissipation. For pipe flow the Nahme number is defined as $\mathrm{Na} = -(4\beta\mu U^2)/k$ where β is the temperature sensitivity of viscosity defined as $-(1/\mu)(\partial\mu/\partial T)$, μ is the viscosity, k is the thermal conductivity, and U is the average fluid velocity in the tube.

Viscous dissipation effects become significant for increasing Na. For the liquids and Reynolds number ranges used in the study by Judy et al. (2002), the largest Nahme number for the presented data was 0.02, and was found for isopropanol. This small Na suggests that for the data presented in that study the viscous dissipation effects were small. Despite this small Na, viscous heating of the fluid can affect the results. Figure 4.12 illustrates the Poiseuille number Po as a function of Reynolds number for a fused silica square micro-channel of length $L = 11.4$ cm and hydraulic diameter $d_\mathrm{h} = 74.1$ μm ($L/d_\mathrm{h} = 1{,}543$) with isopropanol as the working fluid. The maximum rise in liquid temperature for this case was 6.2 K, found at the maximum Reynolds number tested, $\mathrm{Re} \approx 300$. The figure shows Po calculated in two ways: (1) using a viscosity based on the tube inlet temperature, and (2) using a viscosity based on the average of tube inlet and exit temperatures. Note that when the average temperature is used, Po is effectively independent of the Reynolds number. By contrast, when the temperature at the tube inlet is used to evaluate the viscosity, the friction factor drops with increasing Reynolds number, as the effect of viscous heating becomes more pronounced at higher fluid velocities. Even for the small Nahme

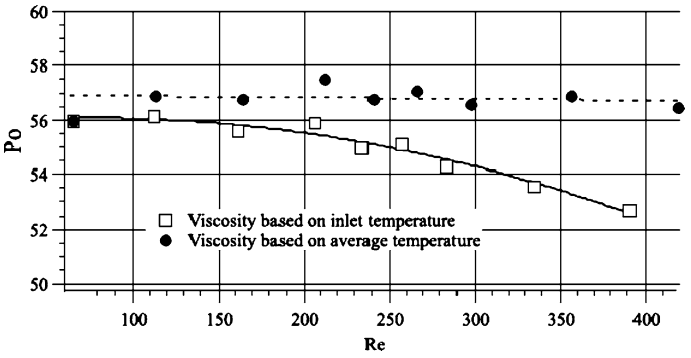

Fig. 4.12 Measured Po vs. Reynolds number with viscosity based on average tube fluid temperature represented by *circles*, and inlet temperature represented by *squares* for a fused silica square micro-channel with isopropanol. Reprinted from Judy et al. (2002) with permission

number characterizing this data set (Na = 0.02), the viscous heating and associated viscosity variation can result in a 7–10% drop in Po. For the small Nahme numbers and associated small rise in mean temperature over tube length found in tests reported here, the average of the fluid temperatures at the tube inlet and exit appears to be an appropriate reference condition for thermophysical properties.

It should be emphasized that under conditions of energy dissipation the definition of the heat transfer coefficient as $k\left(\partial T/\partial r\right)_{r=r_0}/(\overline{T}-T_{\mathrm{w}})$, where $\overline{T}$ is the average fluid temperature and T_{w} is the wall temperature, does not characterize the actual heat transfer properly (Kays and Crawford 1993; Schlichting 2000).

The factors that determine the temperature distribution of the fluid are (1) convective heat transfer, and (2) heat released due to viscous dissipation. For a cooling regime when the fluid temperature at the inlet $T_0 > T_{\mathrm{w}}$, convective heat transfer from the fluid to the wall leads to a decrease in the fluid temperature along a relatively small dimensionless distance X^+. The heat released due to viscous dissipation causes an increase in the fluid temperature. The contribution of each component to the behavior of the fluid temperature depends on X^+. At small X^+ the dominant role belongs to convective heat transfer, whereas at large X^+ the effect of viscous dissipation becomes significant. These two factors determine the specific shape of the temperature distribution along the micro-channel: the fluid temperature variation along the micro-channel has a minimum. It is worth noting that under the condition of viscous dissipation the fluid temperature does not reach the wall temperature at any value of X^+.

For the heating regime at small X^+, the heat transferred from the wall to the cold fluid and the heat released due to viscous dissipation lead to an increase in

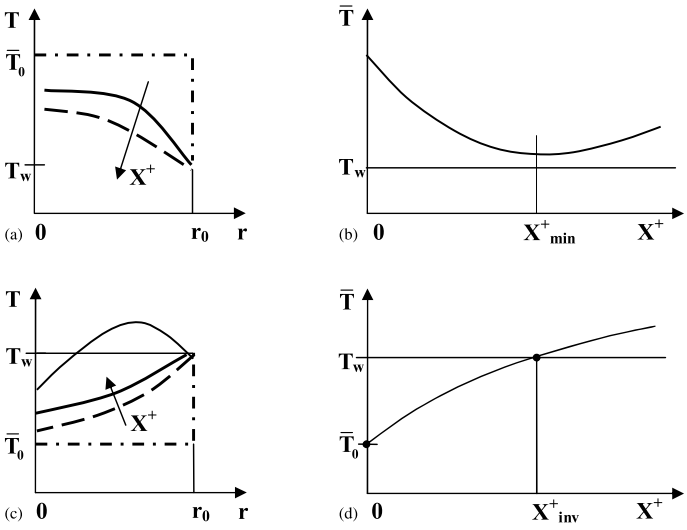

Fig. 4.13a–d Temperature distribution (**a**) and (**b**) $\overline{T}_0 > T_{\mathrm{w}}$, (**c**) and (**d**) $\overline{T}_0 < T_{\mathrm{w}}$. The *dotted line* corresponds to temperature distribution at $X^+ = 0$; the *arrows* show the direction of the increase of X^+. Reprinted with permission from Hetsroni et al. (2005)

fluid temperature. At some value of X^+ the fluid temperature may exceed the wall temperature (Fig. 4.13). The difference $T - T_w$ decreases up to the inversion point $X^+ = X^+_{inv}$. This leads to physically unrealistic results like infinite growth of the Nusselt number in the vicinity of the inversion point.

The analysis of the behavior of the fluid temperature and the Nusselt number performed for a circular tube at the thermal wall boundary condition $T_w = \text{const.}$ also reflects general features of heat transfer in micro-channels of other geometries.

4.4 Axial Conduction

4.4.1 Axial Conduction in the Fluid

This problem was the subject of a number of theoretical investigations carried out for conventional size channels, e.g., Petukhov (1967), Hehnecke (1968), Nguyen (1992), Nguyen et al. (1996), and Weigand and Lauffer (2004). We consider the effect of axial conduction in the fluid on heat transfer in micro-channels. The energy equation is formulated for the flow of an incompressible fluid with constant physical properties. Assuming that the energy dissipation is negligible, we obtain:

$$\rho u c_p \frac{\partial T}{\partial x} = k \left\{ \frac{1}{r} \frac{\partial}{\partial r} \left(r \frac{\partial T}{\partial r} \right) + \frac{\partial^2 T}{\partial x^2} \right\} \tag{4.13}$$

where x and r are the longitudinal and radial coordinates, ρ, c_p and k are the density, specific heat and thermal conductivity of the fluid, respectively.

For $q = \text{const.}$ (q is the heat flux on the wall), we introduce new variables

$$\tilde{u} = \frac{u}{U_{ax}},\ R = \frac{r}{r_0},\ X^+ = \frac{2}{\mathrm{Pe}} \frac{x}{d},\ \theta = \frac{T - T_0}{\left(\frac{qd}{k} \right)} \tag{4.14}$$

where $\mathrm{Pe} = \frac{Ud}{\alpha}$, $\tilde{u} = (1 - R^2)$, $d = 2r_0$, U_{ax} and $U = U_{ax}/2$ are the axial and average velocities, respectively, T_0 is the fluid temperature at the entrance of the heating section, and α is the thermal diffusivity.

The dimensionless form of Eq. (4.13) is:

$$\tilde{u} \frac{\partial \theta}{\partial X^+} = \frac{1}{R} \frac{\partial}{\partial R} \left(R \frac{\partial \theta}{\partial R} \right) + \frac{1}{\mathrm{Pe}^2} \frac{\partial^2 \theta}{\partial X^{+2}}\,. \tag{4.15}$$

Transferring Eq. (4.15) to divergent form and integrating this equation through the micro-channel cross-section we obtain:

$$\frac{\partial}{\partial X^+} \left(\int_0^1 \tilde{u} \theta R \, \mathrm{d}R \right) = \left(R \frac{\partial \theta}{\partial R} \right) \Big|_0^1 + \frac{1}{\mathrm{Pe}^2} \frac{\partial^2}{\partial X^{+2}} \left(\int_0^1 \theta R \, \mathrm{d}R \right). \tag{4.16}$$

Assuming that the exit of the micro-channel is connected to an adiabatic section the boundary conditions are:

$$X^+ = 0\,, \quad \theta = 0\,; \qquad X^+ > 0 \begin{cases} R = 0, & \dfrac{\partial \theta}{\partial R} = 0 \\ R = 1, & \dfrac{\partial \theta}{\partial R} = \dfrac{1}{2} \end{cases}; \qquad X^+ = X_*^+\,, \quad \frac{\partial \theta}{\partial X^+} = 0 \tag{4.17}$$

where X_*^+ corresponds to the micro-channel exit.

Taking into account conditions (4.17) we obtain from (4.16):

$$\frac{\mathrm{d}}{\mathrm{d}X^+}\left(\int_0^1 \tilde{u}\theta R\,\mathrm{d}R\right) = \frac{1}{2} + \frac{1}{\mathrm{Pe}^2}\frac{d^2\overline{\theta}}{\mathrm{d}X^{+2}} \tag{4.18}$$

where $\overline{\theta} = \int_0^1 \theta R\,\mathrm{d}R$ is the average temperature.

Assuming that θ is a weak function of R and $\theta \approx \overline{\theta}$ we can estimate:

$$\int_0^1 \tilde{u}\theta R\,\mathrm{d}R \approx \frac{\overline{\theta}}{4}\,. \tag{4.19}$$

Then Eq. (4.18) becomes

$$\frac{\partial^2\overline{\theta}}{\partial X^{+2}} - \frac{1}{4}\mathrm{Pe}^2\frac{\partial\overline{\theta}}{\partial X^+} + \frac{1}{2}\mathrm{Pe}^2 = 0\,. \tag{4.20}$$

The solution of Eq. (4.20) is:

$$\overline{\theta} = C_1 + C_2\exp\left(\frac{\mathrm{Pe}^2}{4}X^+\right) + 2X^+ \tag{4.21}$$

where C_1 and C_2 are constants.

Using the first and third conditions of (4.17) we find:

$$C_1 = C_2, \quad C_2 = -\frac{2}{\left(\mathrm{Pe}^2/4\right)}\exp\left(-\frac{\mathrm{Pe}^2}{4}X_*^+\right). \tag{4.22}$$

The effect of axial conduction on heat transfer in the fluid in the micro-channel can be characterized by a dimensionless parameter

$$M = \frac{|q_{\mathrm{cond}}|}{|q_{\mathrm{conv}}|} \tag{4.23}$$

that expresses the relation between heat fluxes due to conduction and convection. In Eq. (4.23) $q_{\mathrm{conv}} = \rho U c_{\mathrm{p}}(T - T_0)$, $q_{\mathrm{cond}} = k\frac{\mathrm{d}T}{\mathrm{d}x}$. Substitution of the expression for variable $\overline{\theta}$ and $\frac{\partial\overline{\theta}}{\partial X^+}$ in relation (4.23) gives:

$$M = \frac{1}{4}\frac{1 - \exp(\chi^+ - \chi_*^+)}{\chi^+ - \exp(\chi^+ - \chi_*^+) + \exp(-\chi_*^+)} \tag{4.24}$$

where $\chi^+ = \frac{\mathrm{Pe}^2 X^+}{4}$, $\chi_* = \frac{\mathrm{Pe}^2 X_*^+}{4}$.

The limiting cases are:

$$1.\ \chi^+ \ll 1,\ \chi_*^+ \gg 1$$

$$2.\ \chi^+ - \chi_*^+ \ll 1 \quad \begin{cases} \text{a. } \chi_*^+ \gg 1 \\ \text{b. } \chi_*^+ \ll 1 \end{cases}$$

which correspond to heat transfer at the cooling inlet and heat transfer in the vicinity of the adiabatic outlet, respectively. In the first case we obtain the following evaluation of parameter M:

$$M = \frac{1}{4}\frac{1}{\chi^+} \gg 1\,. \tag{4.25}$$

It shows that close to the micro-channel inlet, heat losses to the cooling inlet due to axial conduction in the fluid are dominant. In the second case parameter M is:

a. Long micro-channel

$$M = \frac{\chi_*^+ - \chi^+}{\chi_*^+ - 1} \ll 1 \tag{4.26}$$

b. Short micro-channel

$$M = \frac{\chi_*^+ - \chi^+}{\chi_*^+} \ll 1 \tag{4.27}$$

Thus, M decreases when χ (and the Peclet number) increases. Accordingly, the Nusselt number decreases when the Peclet number increases, and approaches its limiting value Nu_∞ that corresponds to $\mathrm{Pe} \to \infty$.

The existence of heat transfer due to axial conduction in the fluid leads to increasing difference between wall and fluid temperatures and decreasing value of the Nus-

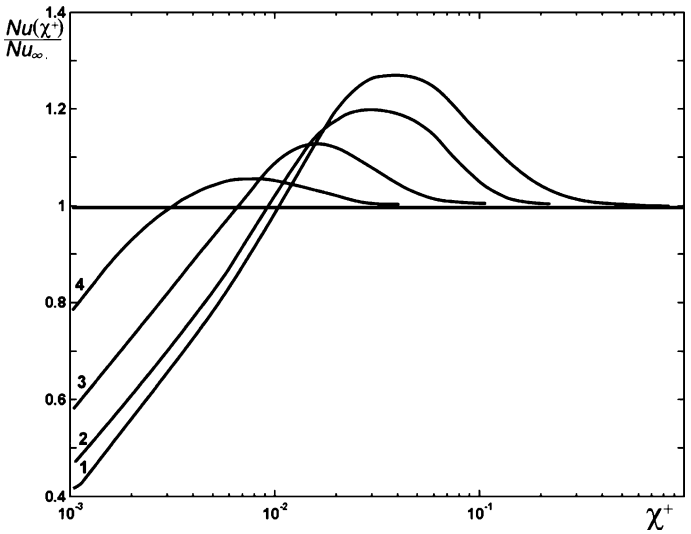

Fig. 4.14 Numerical calculations of the dependences $\mathrm{Nu}(X^+)$: *1* $\mathrm{Pe} = 1$, *2* $\mathrm{Pe} = 2.5$, *3* $\mathrm{Pe} = 10$, *4* $\mathrm{Pe} = 45$

selt number within the entrance section as compared to Nu_∞. These effects are illustrated in Fig. 4.14, which shows the dependence $\mathrm{Nu}(\chi^+)/\mathrm{Nu}_\infty$ on χ^+. It is possible to estimate the critical value of the parameter M that subdivides the states at which the effect of axial conduction dominates ($M > M_{\mathrm{cr}}$) or it is negligible ($M < M_{\mathrm{cr}}$). According to the data of Petukhov (1967), this critical value is $M_{\mathrm{cr}} \simeq 0.01$. In line with these results we obtain the following evaluation of the length where the effect of axial conduction in the fluid should be taken into consideration: $\frac{x}{r_0}\mathrm{Pe} \leq 20$.

4.4.2 Axial Conduction in the Wall

The problem of axial conduction in the wall was considered by Petukhov (1967). The parameter used to characterize the effect of axial conduction is $P = \left(1 - d_0^2/d_{\mathrm{in}}^2\right)(k_2/k_1)$. The numerical calculations performed for $q = \text{const.}$ and neglecting the wall thermal resistance in radial direction, showed that axial thermal conduction in the wall does not affect the Nusselt number Nu_∞. Davis and Gill (1970) considered the problem of axial conduction in the wall with reference to laminar flow between parallel plates with finite conductivity. It was found that the Peclet number, the ratio of thickness of the plates to their length are important dimensionless groups that determine the process of heat transfer.

The effect of axial conduction in the wall on the heat transfer in micro-channels was recently investigated by Maranzana et al. (2004) and Tiselj et al. (2004). In the first study the thermal structure of laminar flow between parallel plates was investigated. In the second one, heat transfer characteristics of water flowing through triangular silicon micro-channels were analyzed. For the physical interpretation of the effects due to axial conduction in the wall, Maranzana et al. (2004) introduced "axial conduction number" M defined as the ratio of conductive heat flux to convective heat flux. Numerical calculations by Maranzana et al. (2004) showed that the effect of axial conduction in the wall is significant when $M > 10^{-2}$ or estimated using relation (Celata et al. 2005, 2006) suggested the relation $k_{\mathrm{w}}\left(d_{\mathrm{out}}^2 - d_0^2\right)/k_{\mathrm{f}}d_0L.01\mathrm{Re}\,\mathrm{Pr}$, where k_{w} and k_{f} are the thermal conductivity of wall and liquid, respectively, d_{out} and d_0 are the outer and inner tube diameter, and L is the tube length. According to Tiselj et al. (2004), axial conduction in the wall significantly affects the longitudinal fluid and wall temperature distribution and longitudinal distribution of the normal and axial heat flux. We will discuss these results in Sect. 4.5.

4.4.3 Combined Axial Conduction in the Fluid and in the Wall

The energy equations for the fluid and the wall are (Petukhov 1967):

$$\frac{\partial \bar{u}\theta_{\mathrm{l}}}{\partial X^+} = \frac{1}{R}\frac{\partial}{\partial R}\left(R\frac{\partial \theta_{\mathrm{l}}}{\partial R}\right) + \frac{1}{\mathrm{Pe}^2}\frac{\partial^2 \theta_{\mathrm{l}}}{\partial X^{+2}} \tag{4.28}$$

$$\frac{1}{R}\frac{\partial}{\partial R}\left(R\frac{\partial\theta_2}{\partial R}\right)+\frac{1}{\mathrm{Pe}^2}\frac{\partial^2\theta}{\partial X^{+2}}=0 \tag{4.29}$$

where $\theta_i=(T_i-T_0)/(qd_1/k_i)$, $i=1,2$ for the fluid and wall, respectively.

Integration of Eqs. (4.28) and (4.29) through the cross-section of the microchannel gives:

$$\frac{\partial}{\partial X^+}\left(\int_0^1\tilde{u}\theta_1R\,\mathrm{d}R\right)=\left(R\frac{\partial\theta_1}{\partial R}\right)\Big|_0^1+\frac{1}{\mathrm{Pe}^2}\frac{\partial^2}{\partial X^{+2}}\left(\int_0^1\theta_1R\,\mathrm{d}R\right) \tag{4.30}$$

$$\left(R\frac{\partial\theta_2}{\partial R}\right)\Big|_1^{R_*}+\frac{1}{\mathrm{Pe}^2}\frac{\partial^2}{\partial X^{+2}}\left(\int_1^{R_*}\theta_2R\,\mathrm{d}R\right)=0 \tag{4.31}$$

where

$$R_*=\frac{r_0}{r_{\mathrm{out}}},\quad \left.\frac{\partial\theta_1}{\partial R}\right|_0=0,\quad \left(\frac{\partial\theta_1}{\partial R}=\frac{\partial\theta_2}{\partial R}\right)\Big|_{R=1}=0,\quad \left.\frac{\partial\theta_2}{\partial R}\right|_{R=R_*}=\frac{k_1}{k_2}\frac{1}{2}. \tag{4.32}$$

The sum of Eq. (4.30) and Eq. (4.31) is:

$$\begin{aligned}&\frac{\partial}{\partial X^+}\left(\int_0^1\tilde{u}\theta_1R\,\mathrm{d}R\right)\\&=\left(R\frac{\partial\theta_2}{\partial R}\right)\Big|_{R=R_*}+\frac{1}{\mathrm{Pe}^2}\frac{\partial^2}{\partial X^{+2}}\left(\int_0^1\theta_1R\,\mathrm{d}R\right)+\frac{1}{\mathrm{Pe}^2}\frac{\partial^2}{\partial X^{+2}}\left(\int_1^{R_*}\theta_2R\,\mathrm{d}R\right)\end{aligned} \tag{4.33}$$

Taking into account that

$$\overline{\theta}_1=\int_0^1\theta_1R\,\mathrm{d}R,\quad \overline{\theta}_2=(R_*^2-1)^{-1}\int_1^{R_*}\theta_2R\,\mathrm{d}R \tag{4.34}$$

we obtain:

$$\frac{\mathrm{d}}{\mathrm{d}X^+}\left(\int_0^1\tilde{u}\theta_1R\,\mathrm{d}R\right)=\frac{k_1}{k_2}\frac{1}{2}+\frac{1}{\mathrm{Pe}^2}\frac{d^2\overline{\theta}_1}{\mathrm{d}X^{+2}}+\frac{(R_*^2-1)}{\mathrm{Pe}^2}\frac{d^2\overline{\theta}_2}{\mathrm{d}X^{+2}}. \tag{4.35}$$

Assuming that $\mathrm{d}^2\overline{\theta}_1/\mathrm{d}X^{+2}\approx\mathrm{d}^2\overline{\theta}_2/\mathrm{d}X^{+2}$ the following equation for average fluid temperature was obtained

$$\frac{\mathrm{d}^2\overline{\theta}_1}{\mathrm{d}X^{+2}}-\frac{\mathrm{Pe}^2}{4R_*^2}\frac{\mathrm{d}\overline{\theta}_1}{\mathrm{d}X^{+2}}+\frac{1}{2}k_{1,2}\frac{\mathrm{Pe}^2}{R_*^2}=0. \tag{4.36}$$

The longitudinal fluid temperature distribution is:

$$\overline{\theta}_1=C_1+C_2\exp\left(\frac{\mathrm{Pe}^2}{4R_*^2}X^+\right)+2\frac{k_1}{k_2}X^+ \tag{4.37}$$

where $C_1=-C_2$; $C_2=-\frac{2(k_1/k_2)}{(\mathrm{Pe}^2/4R_*^2)}\exp\left(\frac{\mathrm{Pe}^2X_*^+}{4R_*^2}\right)$.

Then, the parameter M is

$$M = \frac{1}{4}\frac{1-\exp(\tilde{\chi}-\tilde{\chi}_*)}{(k_1/k_2)\tilde{\chi}-\exp(\tilde{\chi}-\tilde{\chi}_*)+\exp(-\tilde{\chi}_*)} \tag{4.38}$$

where $\tilde{\chi} = \frac{\mathrm{Pe}^2 X^+}{4R_*^2}$, $\tilde{\chi}_* = \frac{\mathrm{Pe}^2 X_*^+}{4R_*^2}$.

For the limiting cases $\tilde{\chi} \ll 1$ and $\tilde{\chi}_* \gg 1$ we obtain the following estimation:

$$M = \frac{1}{4k_{1,2}}\frac{1}{\tilde{\chi}} = \frac{\Lambda}{4\chi^+} \tag{4.39}$$

where $\Lambda = (k_2/k_1)\,(r_0/r_{\mathrm{out}})^2$. For conditions corresponding to flow in micro-channels, this factor is $\Lambda \gg 1$. For example Λ equals 25 and 250 for water flows in micro-channels of $r_0/r_{\mathrm{out}} = 1.1$ made of stainless steel and silicon, respectively. This shows that conduction in the wall has significant effect on the heat transfer in the micro-channels. It can be an important factor that leads to changes in the heat transfer coefficient.

4.5 Micro-Channel Heat Sinks

4.5.1 Three-Dimensional Heat Transfer in Micro-Channel Heat Sinks

The cooling systems fabricated from a large number of rectangular (Qu and Mudawar 2002a; Toh et al. 2002; Li et al. 2004), triangular (Tiselj 2004) or circular (Kroeker et al. 2004) micro-channels were investigated both theoretically and experimentally. The micro-channel heat sinks are highly complicated systems with a non-uniform distribution of thermal characteristics. The existence of a non-uniform temperature field in the liquid and solid substrate leads to a non-uniform distribution of heat fluxes in the streamwise and spanwise direction. Qu and Mudawar (2002a) carried out calculations at Re = 140, 700, and 1,400 for heat sinks. The micro-channels had a width of 57 μm and a depth of 180 μm, and were separated by a 43 μm wall. The major approximations introduced in the classical fin analysis method for micro-channel heat sinks operating in the laminar flow regime are summarized and assessed based on numerical results. The numerical results of that study revealed that the classical fin method could only provide a qualitatively correct picture of the heat transport in a micro-channel heat sink.

Numerical results of the heat transfer inside four 1 cm^2 heat sinks with 150 and 200 channels were presented by Toh et al. (2002). Their calculation predicted the local thermal resistance very well. The micro-heat sink modeled in the numerical investigation by Li et al. (2004) consisted of a 10 mm long silicon substrate. The rectangular micro-channels had a width of 57 μm, and a depth of 180 μm. The heat

transfer calculations were performed for Reynolds numbers of 144, 77 and 42. The longitudinal heat conduction along the silicon wafer at different Reynolds number is different. In reality, because it is difficult to achieve an adiabatic boundary at the inlet and outlet of the heat sink as assumed in the numerical model, a significant portion of the heat is transferred to the inlet and outlet manifolds, especially for low fluid flow conditions. Thus, when evaluating the heat transfer in micro-heat sinks with low fluid flow rates, particular attention should be paid to the effects of heat conduction through the wafer.

Kroeker et al. (2004) investigated thermal characteristics of heat sinks with circular micro-channels using the continuum model based on the conventional Navier–Stokes equations and the energy conservation equation. Developing flow (both hydrodynamically and thermally) was assumed in the flow region and three-dimensional conjugate heat transfer was assumed in the solid region. At the inlet and outlet of the solid region (copper or silicon), adiabatic boundary conditions were imposed. The calculations of local Nusselt number performed at Re = 500 and Re = 1,000 follow closely the classical solution reported by Shah and London (1978) for forced convection in tubes with constant wall temperature.

One particular characteristic of conduction heat transfer in micro-channel heat sinks is the strong three-dimensional character of the phenomenon. The smaller the hydraulic diameter, the more important the coupling between wall and bulk fluid temperatures, because the heat transfer coefficient becomes high. Even though the thermal wall boundary conditions at the inlet and outlet of the solid wall are adiabatic, for small Reynolds numbers the heat flux can become strongly non-uniform: most of the flux is transferred to the fluid at the entrance of the micro-channel. Maranzana et al. (2004) analyzed this type of problem and proposed the model of channel flow heat transfer between parallel plates. The geometry shown in Fig. 4.15 corresponds to a flow between parallel plates, the uniform heat flux is imposed on the upper face of block 1; the lower face of block 0 and the side faces of both blocks

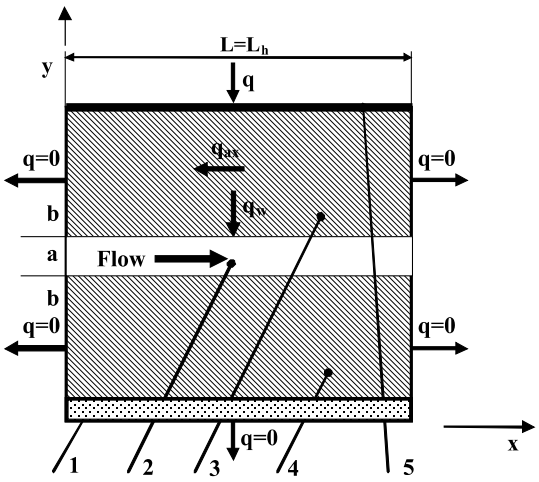

Fig. 4.15 Effect of axial conduction, channel between two parallel plates (Maranzana et al. 2004) (schematic view): *1* cover plate, *2* micro-channel, *3* silicon block 1, *4* silicon block 0, *5* heater

are adiabatic. The two 10 mm long and 500 μm thick blocks are made of silicon, water flows in the 100 μm thick channel. Figure 4.16a–c shows interface temperature, interface heat flux and the Nusselt number. The lower the Reynolds number, the larger the axial conduction effects.

The numerical and experimental study of Tiselj et al. (2004) (see Fig. 4.17) was focused on the effect of axial heat conduction through silicon wafers on heat transfer in the range of Re = 3.2−84. Figure 4.17 shows their calculation model of a triangular micro-channels heat sink. The results of calculations are presented in Fig. 4.18.

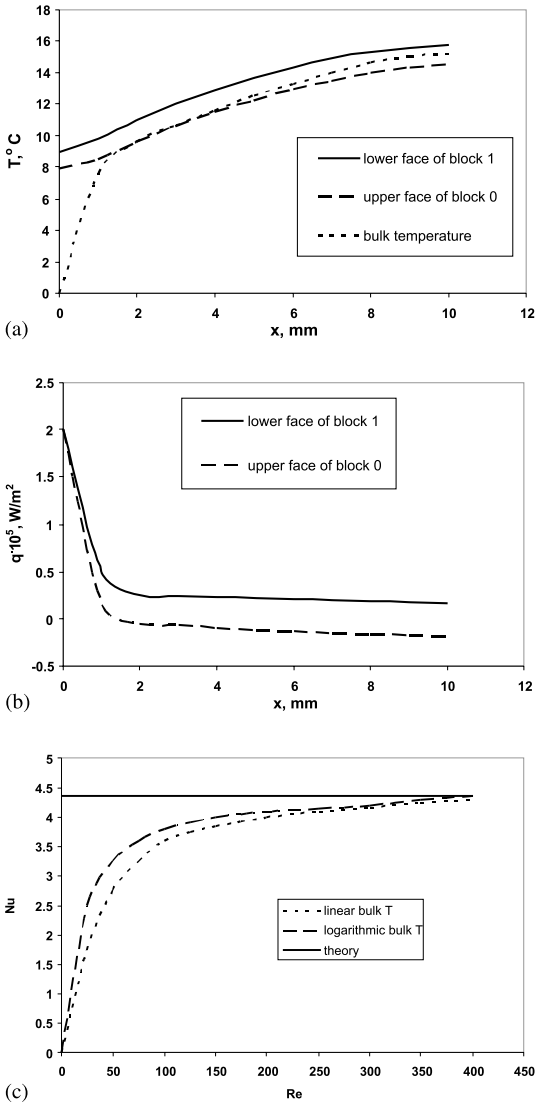

Fig. 4.16a–c Effect of axial conduction. Numerical simulation. (**a**) Interface temperature. (**b**) Interface heat flux. (**c**) The Nusselt numbers. Reprinted from Maranzana et al. (2004) with permission

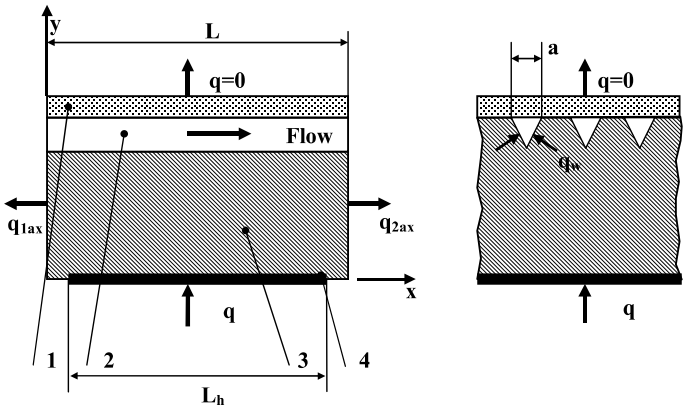

Fig. 4.17 Calculation model of triangular micro-channels heat sink: *1* cover plate, *2* micro-channel, *3* silicon wafer, *4* heater. Reprinted from Tiselj et al. (2004) with permission

The thermal wall boundary conditions used by Tiselj et al. (2004) at the inlet and outlet of the solid wall are not adiabatic (cf. Maranzana et al. 2004). The heat sink was made from a square-shaped silicon substrate of 15×15 mm and 530 μm thick, and in the silicon substrate, 17 parallel micro-channels were etched. The cross-section of each channel was an isosceles triangle with a base of 310 μm, the length of the micro-channels was $L = 15$ mm, the heating length was $L_h = 10$ mm. The angles at the base were 55°, the hydraulic diameter was $d_h = 160$ μm. The experimental results were used for numerical calculation. The bulk water temperature and the inner heated wall temperature are shown in Fig. 4.18a. Both temperatures did not change linearly along the longitudinal direction. In fact, a linear temperature rise cannot be regarded as a good approximation for both temperatures. When axial heat flux is directed to both the inlet and the outlet manifolds, the water and heated surface temperatures did not change monotonically. The longitudinal distributions of wall normal heat fluxes are presented in Fig. 4.18b. The heat fluxes are taken to be positive if they are directed from the solid to the fluid, and negative otherwise. The direction and the magnitude of the negative heat flux depend on relation between the two thermal resistances: the first defines the heat transport from the wall through the boundary layer to the fluid core, and the second one quantifies the possibility of heat transport through the silicon wafer. The importance of the second alternative pathway for the heat transfer can be truly appreciated only in a three-dimensional conjugate heat transfer problem. The thermal wall boundary conditions have a dominant role in such a problem. Numerical predictions of the local Nusselt number variation in the streamwise direction are plotted in Fig. 4.18c. As indicated by Incropera and De Witt (1996) the thermal entry length of a circular tube is:

$$L_{\text{therm}} = 0.05\text{Pe} \cdot d_h \,. \tag{4.40}$$

In the study by Tiselj et al. (2004), the thermal entry length was 0.13 and 3.3 mm for $\text{Re} = 3.2$ and 84, respectively.

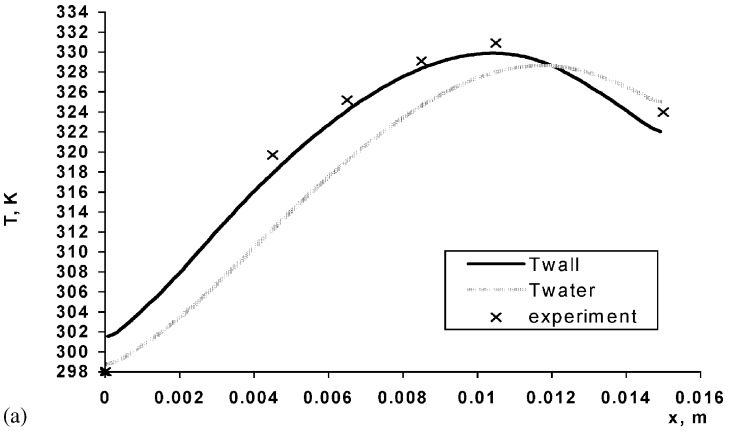

(a)

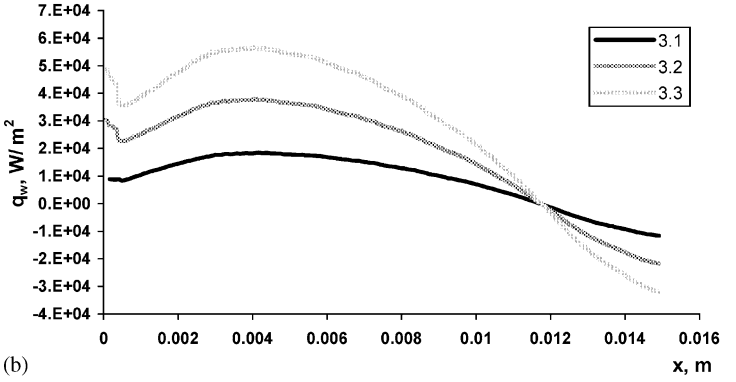

(b)

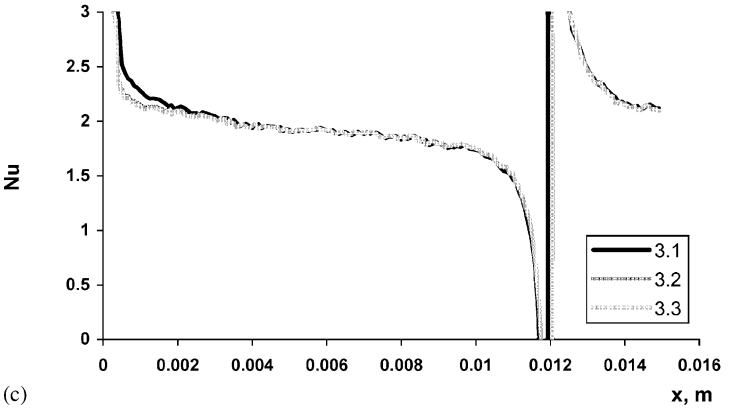

(c)

Fig. 4.18a–c Effect of axial conduction. Triangular micro-channels. $\dot{m} = 0.0356$ g/s. (**a**) Average water and silicon temperature distributions. $N = 8.424$ W. (**b**) Wall normal heat flux distribution in the silicon chip. 3-1 $N = 2.816$ W, 3-2 $N = 5.676$ W, 3-3 $N = 8.424$ W. (**c**) Axial distribution of the Nusselt number in the chip. 3-1 $N = 2.816$ W, 3-2 $N = 5.676$ W, 3-3 $N = 8.424$ W. Reprinted from Tiselj et al. (2004) with permission

4.5.2 Entrance Effects

The entrance effects in a single channel were extensively studied in the past (Petukhov 1967; Kays and Crawford 1993; Baehr and Stephan 1998; Schlichting 2000; Toh et al. 2002; Gamart et al. 2005). We restrict our discussion to the effect of inlet and the outlet manifolds on the flow and temperature distributions between the parallel micro-channels. Hetsroni et al. (2001) and Klein et al. (2005) observed an uneven liquid distribution in the parallel micro-channels. Depending on the particular manifold design, the difference between the flow rates into some parallel micro-channels was up to about 20%. Furthermore, due to relatively high thermal conductivity of the manifolds, fluid pre-warming occurred in the inlet manifold and additional warming occurred in the outlet manifold. The behavior of the Nusselt number depends, at least partly, on the entrance effects, which may be important in the laminar regime. The problem was also studied by Gamart et al. (2005). Idealizing the flow rate as uniform can result in a significant error when predicting the temperature distribution of a heated electronic device. Lee et al. (2005) showed that the entrance and boundary conditions imposed in the experiment need to be carefully matched in the predictive approaches. In this case numerical predictions based on a classical, continuum approach were in good agreement with the experimental data.

4.5.3 Characteristic Parameters

Two definitions were considered by Qu and Mudawar (2004) for heat flux to the heat sink. The first is an "effective" heat flux defined as the total electrical power input divided by the top area of the heat sink. The second definition is a mean heat flux averaged over the micro-channel heated inside area. We determine heat flux as the power calculated from the energy balance based on fluid temperature at the inlet and outlet manifolds, divided by the heated area of the micro-channel side walls (Tiselj et al. 2004). Often special effects are proposed to explain unexpected experimental results. A common assumption often made (Wang and Peng 1994; Peng and Peterson 1995; Peng and Peterson 1996) is to consider the wall heat flux to be uniform along the channels. However, according to Fig. 4.16b, the wall heat flux was far from uniform. As shown in Figs. 4.6c and 4.16a, the bulk temperature of the fluid did not vary linearly (Gao et al. 2002; Maranzana et al. 2004; Tiselj et al. 2004). This effect is especially important when the M number is large. For example, Maranzana et al. (2004) utilized exact modeling of heat conduction in the wall. The corresponding simulated estimation of the convective heat transfer coefficient at $M = 0.32$ was equal to $25{,}900\,\mathrm{W/m^2\,K}$. By comparison, the one-dimensional model, assuming that the bulk temperature is linear, yields a mean convective heat transfer coefficient of $6{,}100\,\mathrm{W/m^2\,K}$. Axial conduction can be neglected for M number lower than 0.01.

4.5.4 Effect of Wall Roughness

Wall roughness leads to increasing friction factor at the same Reynolds number. Existence of roughness leads also to a decrease in the value of the critical Reynolds number, at which the transition from laminar to turbulent flow occurs. We suggested a following estimation of the relative roughness, corresponding to the hydrodynamic threshold that subdivides the flow in smooth and rough channels (Hetsroni 2005): $k_s/r_0 < 5/1.41\mathrm{Re}^{0.5}$, where k_s is the average height of roughness, r_0 is the channel hydraulic radius, and Re is the Reynolds number. For Re $\sim$ 2,000, the relative roughness that corresponds to the boundary between the smooth and rough channels is about 0.08. Turner et al. (1999, 2000) concluded that micro-channel surfaces with relative surface roughness of 0.06 did not cause any statistical change in the friction factor for laminar flow. The effect of surface roughness on heat transfer depends on the Prandtl number. Kandlikar et al. (2003) reported that for a 1,067 μm diameter tube, the effect of relative roughness of about 0.003 on heat transfer in water flow was insignificant. For 620 μm, the same relative roughness increases the heat transfer. New experiments should be performed to clarify the effect of wall roughness on heat transfer.

4.5.5 Interfacial Effects

Turner et al. (1999) reported that for the Knudsen number Kn < 0.04 (ratio of mean free path to channel hydraulic diameter) the continuum-based equations can be used for flow in micro-channels. Because the micro-devices have a large surface-to-volume ratio, factors related to surface effects have more impact on the flow at small scales. Among these are the surface electrostatic charges. If the liquid contains even a small amount of ions, the electrostatic charges on the solid surface will attract the counter-ions in the fluid to establish an electrical field. The arrangement of the electrostatic charges on the solid surface and the balancing charges in the liquid is called the electrical double layer (EDL). Mala et al. (1997b), Yang and Li (1998), and Ren et al. (2001) reported numerical and experimental results for the EDL effect with different liquids. They found that the EDL effect led to higher friction coefficient for pure water and dilute solutions. No results for heat transfer were presented.

4.5.6 Effect of Measurement Accuracy

In experiments of flow and heat transfer in micro-channels, some parameters, such as the Reynolds number, heat transfer coefficient, and Nusselt number, are difficult to obtain with high accuracy. The channel hydraulic diameter measurement error may play a very important role in the uncertainty of the friction factor (Hetsroni

et al. 2005). The analysis carried out by Hetsroni et al. (2003) for micro-tubes reveals the following values of standard uncertainties: for infrared measurements, systematic error 0.1 K, random error 0.2 K; for thermocouples, systematic error 0.1 K, random error 0.15 K; for temperature acquisition system, systematic error 0.1 K, random error 0.16 K. The 95% confidence uncertainty of the heat transfer coefficient was 13.2%. The uncertainty must be taken into account in the presentation of experimental data and in comparison between experimental results and theoretical predictions.

4.6 Compressibility Effects

Two-dimensional compressible momentum and energy equations were solved by Asako and Toriyama (2005) to obtain the heat transfer characteristics of gaseous flows in parallel-plate micro-channels. The problem is modeled as a parallel-plate channel, as shown in Fig. 4.19, with a chamber at the stagnation temperature T_{stg} and the stagnation pressure P_{stg} attached to its upstream section. The flow is assumed to be steady, two-dimensional, and laminar. The fluid is assumed to be an ideal gas. The computations were performed to obtain the adiabatic wall temperature and also to obtain the total temperature of channels with the isothermal walls. The governing equations can be expressed as

$$\frac{\partial \rho u}{\partial x} + \frac{\partial \rho v}{\partial y} = 0 \tag{4.41}$$

$$\frac{\partial \rho uu}{\partial x} + \frac{\partial \rho uv}{\partial y} = -\frac{\partial P}{\partial x} + \mu\left(\frac{\partial^2 u}{\partial x^2} + \frac{\partial^2 u}{\partial y^2}\right) + \frac{\mu}{3}\frac{\partial}{\partial x}\left(\frac{\partial u}{\partial x} + \frac{\partial v}{\partial y}\right) \tag{4.42}$$

$$\frac{\partial \rho uv}{\partial x} + \frac{\partial \rho vv}{\partial y} = -\frac{\partial P}{\partial y} + \mu\left(\frac{\partial^2 v}{\partial x^2} + \frac{\partial^2 v}{\partial y^2}\right) + \frac{\mu}{3}\frac{\partial}{\partial y}\left(\frac{\partial u}{\partial x} + \frac{\partial v}{\partial y}\right) \tag{4.43}$$

$$\frac{\partial \rho uh}{\partial x} + \frac{\partial \rho vh}{\partial y} = -P\left(\frac{\partial u}{\partial x} + \frac{\partial v}{\partial y}\right) + k\left(\frac{\partial^2 T}{\partial x^2} + \frac{\partial^2 T}{\partial y^2}\right) + \phi \tag{4.44}$$

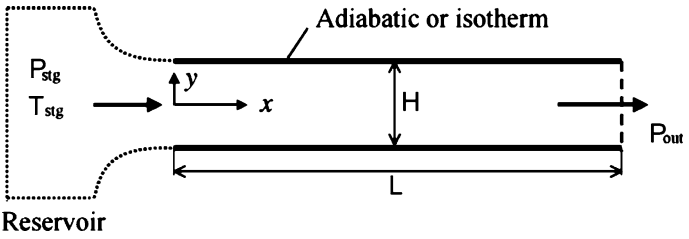

Fig. 4.19 A schematic diagram of parallel-plate micro-channels. Reprinted from Asako and Toriyama (2005) with permission

where

$$\phi = 2\mu\left(\left(\frac{\partial u}{\partial x}\right)^2 + \left(\frac{\partial v}{\partial y}\right)^2\right) - \frac{2\mu}{3}\left(\frac{\partial u}{\partial x} + \frac{\partial v}{\partial y}\right)^2 + \mu\left(\frac{\partial u}{\partial x} + \frac{\partial v}{\partial y}\right)^2. \quad (4.45)$$

The equation of the state for the ideal gas is expressed by

$$h = \frac{\gamma}{\gamma - 1}\frac{P}{\rho} = \frac{\gamma R}{\gamma - 1}T \quad (4.46)$$

where $\gamma = C_p/C_v$, R is the gas constant.

If the range of the channel height is limited to be above 10 μm, then the no-slip boundary condition can be adopted. Furthermore, with the assumptions of uniform inlet velocity, pressure, density, and specified pressure P_{out} at the outlet, the boundary conditions can be expressed as follows:

$$\begin{aligned} &\text{On the walls } (y = \pm 0.5H): && u = v = 0 \\ &\text{At the inlet } (x = 0): && u = u_{in}, v = 0, P = P_{in}, \rho = \rho_{in} \\ &\text{At the outlet } (x = \ell): && P = P_{out}. \end{aligned} \quad (4.47)$$

The thermal boundary conditions on the channel walls are

$$\frac{\partial T}{\partial y} = 0 \text{ for the adiabatic channel} \quad (4.48)$$

$$T = T_w \text{ for the isothermal channel.} \quad (4.49)$$

Adiabatic wall temperature

The computations were performed for air of $R = 287\,\mathrm{J/kg\,K}$, $\gamma = 1.4$, $\mu = 1.862 \times 10^{-5}\,\mathrm{Pa\,s}$, and $k = 0.0261\,\mathrm{W/m\,K}$ to obtain the adiabatic wall temperature. The adiabatic wall temperature is a wall temperature of the channel with the adiabatic walls. The channel height ranged from 10 to 100 μm and length was fixed at 30 mm. The stagnation temperature was kept at $T_{stg} = 300\,\mathrm{K}$. The stagnation pressure P_{stg} varied between 1.3×10^5 and $2.5 \times 10^6\,\mathrm{Pa}$. The outlet pressure was maintained at atmospheric condition $P_{out} = 10^5\,\mathrm{Pa}$.

Since the kinetic energy is related to Ma^2, the adiabatic wall temperature might be reduced by a function of Ma^2 for the cases where the viscous heat dissipation is negligibly small. Then, the values of T_w/T_{stg} for all channels are plotted as a function of Ma^2 in Fig. 4.20.

Channels with isothermal walls

The computations were also performed for the channels with isothermal walls of $T_w = 305$, 310, and 350 K. Air was assumed for the working fluid and the identical thermophysical properties mentioned earlier were used. The channel height ranged from 10 to 100 μm and the ratio of the channel length to its height was either 100 or 200. The stagnation temperature was kept at $T_{stg} = 300\,\mathrm{K}$. The stagnation pressure

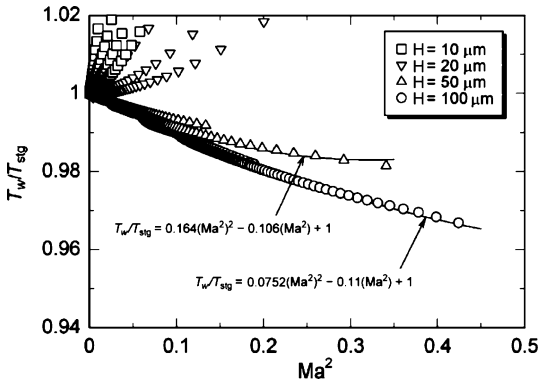

Fig. 4.20 T_w/T_{stg} as a function of Ma^2. Reprinted from Asako and Toriyama (2005) with permission

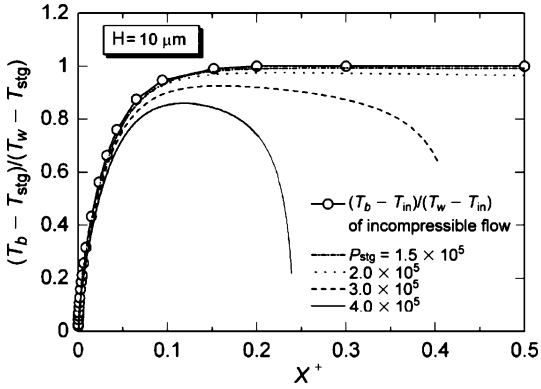

Fig. 4.21 Bulk temperature for $H = 10\,\mu m$ and $T_w = 350$ K. Reprinted from Asako and Toriyama (2005) with permission

P_{stg} was varied between 1.2×10^5 and 4×10^5 Pa. The outlet pressure was maintained at atmospheric condition $P_{out} = 10^5$ Pa.

The values of $(T_b - T_{stg})/(T_w - T_{stg})$ for the channel of $H = 10\,\mu m$ and $T_w = 350$ K are plotted as a function of X^+ in Fig. 4.21 with the bulk temperature for the incompressible flow. The value of the bulk temperature for the incompressible flow is normalized as $(T_b - T_{in})/(T_w - T_{in})$. As seen in the figure, the bulk temperature of the gaseous flow increases along the channel downstream and then levels off. It decreases when approaching the outlet due to conversion of the thermal energy into the kinetic energy. The same trend can be seen for the channels of $h = 20$, 50, and 100 μm. Therefore, the bulk temperature of the gas flow in the micro-channel cannot be estimated from the correlation for the incompressible flow.

4.7 Electro-Osmotic Heat Transfer in a Micro-Channel

Electro-osmosis generated flows are interesting for micro-electronics, biomedical diagnostic techniques, and a number of other applications. Important results related to heat transfer in such flows were obtained recently by Maynes and Webb

(2003) and Horiuchi and Dutta (2004). Below we follow the first of these works and consider some results corresponding to fully developed electro-osmotic heat transfer in circular micro-tubes. At the assumption of no pressure-driven contribution to the velocity field, constant electrical and thermal conductivities and constant wall ζ-potential, the momentum and energy equations that describe flow in circular micro-tubes are

$$\mu \frac{1}{r}\frac{\mathrm{d}}{\mathrm{d}r}\left(r\frac{\mathrm{d}u}{\mathrm{d}r}\right) + \frac{\varepsilon}{r}\frac{\mathrm{d}}{\mathrm{d}r}\left(r\frac{\mathrm{d}\psi}{\mathrm{d}r}\right)\frac{\mathrm{d}\Phi}{\mathrm{d}x} = 0 \tag{4.50}$$

$$\frac{\partial^2 T}{\partial x^2} + \frac{1}{r}\frac{\partial}{\partial r}\left(r\frac{\partial T}{\partial r}\right) = \frac{u}{\alpha}\frac{\partial T}{\partial x} - \frac{s}{k} \tag{4.51}$$

where u and T are the velocity and temperature, Φ is the applied potential field, s is the volumetric energy generation ($s = i_e^2\sigma$, i_e is the conduction current density, σ is the liquid electrical resistivity), ε is the fluid dielectric constant, ψ is the excess charge distribution, k is the thermal conductivity, α is the thermal diffusivity, and μ is the viscosity.

For low wall potentials the Debye–Huckel linearization holds and the excess charge distribution is

$$\psi = \zeta \frac{I_0(r/\lambda)}{I_0(r_0/\lambda)} \tag{4.52}$$

where ζ is the zeta potential, λ is the Debye length, r_0 is the micro-channel radius, and I_0 is the modified Bessel function of the first kind of order zero.

Integration of Eqs. (4.50) and (4.51), with correlation (4.52), yields the following expression for velocity and temperature distribution, at $q_w = \text{const.}$:

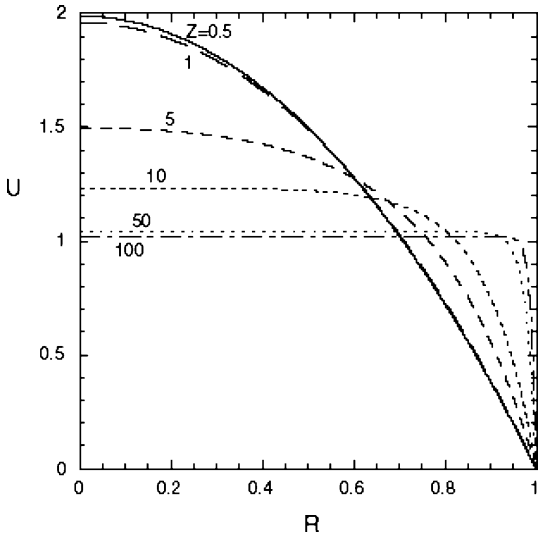

Fig. 4.22 Normalized electro-osmotically driven velocity profiles as a function of z for circular tube. Reprinted from Maynes and Webb (2003) with permission

$$\frac{u}{u_{\max}} = \left[1 - \frac{I_0(ZR)}{I_0(Z)}\right] \tag{4.53}$$

$$\overline{U}_{\max} = \frac{U}{u_{\max}} = \left[1 - \frac{2I_1(Z)}{ZI_0(Z)}\right] \tag{4.54}$$

$$\theta(R) = \left\{\frac{2}{\overline{U}_{\max}} + S\left(\frac{1}{\overline{U}_{\max}} - 1\right)\right\}\left[\frac{R^2-1}{4} + \frac{1}{8\overline{U}_{\max}}\right] \tag{4.55}$$
$$+ \frac{(2+S)}{Z^2\overline{U}_{\max}}\left[1 - \frac{I_0(ZR)}{I_0(Z)}\right] - \frac{(2+S)}{\overline{U}^2_{\max}}C_1(Z) + \frac{S}{\overline{U}_{\max}}C_2(Z)$$

where $R = r/r_0$, $Z = r_0/\lambda$, λ is the Debye length, $\overline{U}_{\max}$ is the maximum possible electro-osmotic velocity for a given applied potential field, $\theta - (T - Tm)(q_w r_0/k)$ is the dimensionless temperature, T_m is the mixed mean temperature, q_w is the wall heat flux, $S = sr_0/q_w$ is the dimensionless energy generation, $\overline{u}$ is the average velocity,

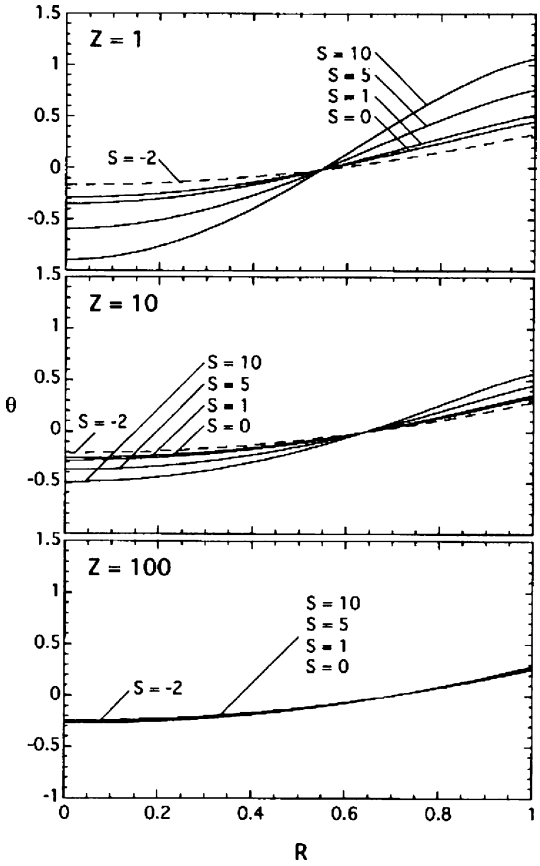

Fig. 4.23 Normalized temperature profile for the circular tube as a function of R and Z. Reprinted from Maynes and Webb (2003) with permission

$$C_1(Z) = \frac{1}{Z^2}\left[3 - \frac{2I_1(Z)}{I_0(Z)} - \frac{I_1^2(Z)}{I_0^2(Z)} - \frac{4I_1(Z)}{zI_0(Z)}\right], \quad C_2(Z) = \frac{1}{Z^2}\left[1 - \frac{2I_1(Z)}{ZI_0(Z)}\right],$$

and I_1 is the modified Bessel function of the first kind of order one.

The velocity and temperature distributions in a cross-section of a circular microtube are plotted in Figs. 4.22 and 4.23. It is seen that the velocity profile is determined by a single parameter, Z, whereas the temperature profile depends on two dimensionless groups, Z and S.

The shape of the velocity profile changes from parabolic corresponding to Poiseuille flow ($Z < 1$) to a uniform, slug-like one which is typical for flow with concentrated momentum source near the wall ($Z \gg 1$) and thin boundary layer. As can be seen in Fig. 4.23, the temperature distribution is independent from parameter s at large enough values of the ratio of micro-channel radius to the Debye length. Taking into account that the Debye length in pure water is about 1 μm (Hunter 1981), it is possible to estimate the micro-channel diameter, at which the electro-osmotic effect on heat transfer is negligible, as about 200 μm.

A general case of heat transfer under the conditions of combined action of electro-osmotic forces and imposed pressure gradient was considered by Chakraborty (2006). The analysis showed that in this case the Nusselt number depends not only on parameters z and S, but also on an additional dimensionless group, which is a measure of the relative significance of the pressure gradient and osmotic forces.

4.8 Closing Remarks

Heat transfer in micro-channels occurs under superposition of hydrodynamic and thermal effects, determining the main characteristics of this process. Experimental study of the heat transfer in micro-channels is problematic because of their small size, which makes a direct diagnostics of temperature field in the fluid and the wall difficult. Certain information on mechanisms of this phenomenon can be obtained by analysis of the experimental data, in particular, by comparison of measurements with predictions that are based on several models of heat transfer in circular, rectangular and trapezoidal micro-channels. This approach makes it possible to estimate the applicability of the conventional theory, and the correctness of several hypotheses related to the mechanism of heat transfer. It is possible to reveal the effects of the Reynolds number, axial conduction, energy dissipation, heat losses to the environment, etc., on the heat transfer.

Theoretical models used for this purpose can be subdivided into two groups depending on the degree of accuracy of their assumptions. The first of these groups includes the simplest one-dimensional models assuming uniform heat flux, constant heat transfer coefficient, etc. The comparison of these models with experiments shows significant discrepancy between the measurements and the theoretical predictions. Using some “new effects,” which are not accounted for by conventional Navier–Stokes and energy equations, the simple models may explain experimental

results. The second group is based on numerical solution of full Navier–Stokes and energy equations, which account for the real geometry of the micro-channel, axial conduction in the fluid and wall, energy dissipation, non-adiabatic thermal boundary condition at the inlet and outlet of the heat sink, dependence of physical properties of fluid on temperature, etc. These models demonstrate a fairly good agreement with available experimental data. As a rule, the numerical calculations using simple models were performed for the following hydraulic boundary conditions:

1. A uniform velocity profile was set at the channel inlet.
2. The flow was assumed to be fully developed in the test section.
3. All the fluid properties were constant.

The thermal boundary conditions were set as follows:

1. Constant heat flux at the walls
2. Adiabatic conditions at the inlet and outlet

These boundary conditions are not in agreement with experiments for which the "new effects" were assumed. As a result, some researchers concluded that conventional Navier–Stokes and energy equations are not valid, and that only "new effects" can explain the experimental data. The numerical solutions based on the Navier–Stokes and energy equations with the proper boundary conditions demonstrate a fairly good agreement with available experimental data. The results can be generalized as follows:

1. The effect of energy dissipation on heat transfer in micro-channels is negligible under typical flow conditions.
2. Axial conduction in the fluid and wall affects significantly the heat transfer in micro-channels. In laminar flow, two heat transfer regimes may be considered. The first takes place when $\mathrm{Re} > 150$ and the axial conduction number $M < 0.01$, or estimated using the relation $k_\mathrm{w}\left(d_\mathrm{out}^2 - d_0^2\right)/k_\mathrm{f} d_0 L.01\mathrm{Re}\,\mathrm{Pr}$. Under these conditions the heat transferred through the solid substrate may be neglected and adiabatic boundary conditions may be imposed at the inlet and outlet manifolds to solve a conjugate three-dimensional heat transfer problem. The second regime occurs at $\mathrm{Re} < 150$, $M > 0.01$. In this case, the heat transferred through the solid substrate should be taken into account.
3. The following considerations must be taken into account in the evaluation of any experimental results:
   a. The experimental results based on the measurements of the fluid temperature only at the inlet and the outlet manifolds of the heat sink may lead to incorrect values of the Nusselt number.
   b. Since it is difficult to measure the local heat flux at the inner channel wall, the definition of the heat transfer coefficient is very important and will strongly influence its value.
4. Accurate estimation of the heat transferred through the solid substrate in experiments should be obtained from energy balance that includes electric power (simulating the electronic components on the top or bottom wall of the heat

sink), convective heat transfer to the fluid (based on fluid mass flow rate and bulk fluid temperature measured at the inlet and outlet manifolds), and heat losses.
5. The heat transfer coefficient calculated numerically using an exact model with regard to the heat transferred through the solid substrate represents the correct variation of the Nusselt number with respect to the Reynolds number.
6. The thermal entry length should be considered by comparison between experimental and numerical results.

Summary

1. A variety of studies can be found in the literature for the solution of the convection heat transfer problem in micro-channels. Some of the analytical methods are very powerful, computationally very fast, and provide highly accurate results. Usually, their application is shown only for those channels and thermal boundary conditions for which solutions already exist, such as circular tube and parallel plates for constant heat flux or constant temperature thermal boundary conditions. The majority of experimental investigations are carried out under other thermal boundary conditions (e.g., experiments in rectangular and trapezoidal channels were conducted with heating only the bottom and/or the top of the channel). These experiments should be compared to solutions obtained for a given channel geometry at the same thermal boundary conditions. Results obtained in devices that are built up from a number of parallel micro-channels should account for heat flux and temperature distribution not only due to heat conduction in the streamwise direction but also conduction across the experimental set-up, and new computational models should be elaborated to compare the measurements with theory.
2. A number of physical parameters or dimensionless groups formulated to describe the same phenomenon have different interpretations. For example, in some studies heat flux is defined as based on a planform area of heat sink top surface, and in other studies as based on a channel heated inside area. The Nusselt number is defined in the literature as based on the difference between wall and fluid temperature. It may be for developed or developing flows, and may present a peripheral local or average value. Additionally this temperature difference may be defined differently. For example, the averaged Nu in micro-channels may be based on the difference $(T_{\mathrm{w,av}} - T_{\mathrm{f,av}})$ where $T_{\mathrm{w,av}}$ is the average temperature of the channel bottom, or averaged peripheral temperature, or may be based on the logarithmic temperature difference, etc. For the most part the temperature $T_{\mathrm{f,av}}$ was defined as $(T_{f,\mathrm{in}} + T_{f,\mathrm{out}})/2$. Such an assumption of linear varying the fluid temperature along a micro-channel may lead to the conclusion which is not physically sound, that the Nusselt number depends on the Reynolds number under laminar flow. An effort to standardize the definitions of physical parameters and dimensional groups for flow through micro-channels should be made.

3. Only a small number of solutions for the laminar forced convection problem and experimental investigations are available in the literature with some variations in the associated thermophysical properties. To the authors' knowledge, for example, no experimental study is available to clarify the effect of the Prandtl number on the heat transfer in micro-channels with different duct geometries.
4. Depending on the particular design of inlet and outlet manifolds, the difference between the flow rates into some parallel micro-channels may be up to 20%. Idealizing the flow rate as uniform can result in significant error in prediction of the temperature distribution of a heated electronic device.
5. For channels above $d_h = 1$ mm the surface roughness generally does not affect the Nusselt number as long as the height of the relative average surface roughness is less than 1%. For small diameters tubes ($d_h < 0.6$ mm) the relative average roughness $k_s/d_h > 0.003$ increases heat transfer up to 25–30% in the range of $Re = 1{,}000-2{,}000$. This effect is more pronounced at higher values of relative surface roughness and Reynolds numbers.

References

Adams TM, Abdel-Khalik SI, Jeter SM, Qureshi ZH (1998) An experimental investigation of single-phase forced convection in micro-channels. Int J Heat Mass Transfer 41:851–857

Asako Y, Toriyama H (2005) Heat transfer characteristics of gaseous flows in micro-channels. Microscale Thermophys Eng 9:15–31

Baehr HD, Stephan K (1998) Heat and mass transfer. Springer, Berlin Heidelberg New York

Bailey DK, Ameel T, Warrington RO, Savoie TI (1995) Single phase forced convection heat transfer in micro-geometries: a review. In: Proceedings the 13th of Intersociety Energy Conversion Engineering Conference, San Diego, 20–25 August 1978. American Society of Mechanical Engineers, New York, pp 301–310

Bastanjian SA, Merzhanov AG, Xudiaev SI (1965) On hydrodynamic thermal explosion. Sov Phys Docl 163:133–136

Celata GP, Como M, Zummo G (2004) Thermal-hydraulic characteristics of single-phase flow in capillary pipes. Exp Thermal Fluid Sci 28:87–95

Celata GP, Cumo M, Marconi V, McPhail SJ, Zummo Z (2005) Micro-tube heat transfer scaling effects: an experimental validation. In: Proceedings of ECI International Conference on Heat Transfer and Fluid Flow in Microchannels, Caste/Vecchio Pascoli, Italy, 25–30 September 2005

Celata GP, Cumo M, Marconi V, McPhail SJ, Zummo Z (2006) Micro-tube liquid single phase heat transfer in laminar flow. Int. J. Heat Mass Transfer 49:3538–3546

Chakraborty S (2006) Analytical solutions of Nusselt number for thermally fully developed flow in microtubes under a combined action of electroosmotic forces and imposed gradients. Int J Heat Mass Transfer 49:810–813

Choi SB, Barron R, Warrington RQ (1991) Fluid flow and heat transfer in micro-tubes. In: Choi D et al. (eds) Micro-mechanical sensors, actuators and systems. ASME DSC 32:121–128

Davis EJ, Gill WN (1970) The effect of axial conduction in the wall on heat transfer with laminar flow. Int J Heat Mass Transfer 23:459–470

Dittus FW, Boelter LMK (1930) Heat transfer in automobile radiators of tubular type. University of California, Berkley. Publ Eng 2(13):443–461

Eckert E, Weise W (1941) Die Temperatur unbeheizter Körper in einem Gasstrom hoher Geschwindigkeit. Forsch Ing Wes 12:40–50

Gad-el-Hak M (1999) The fluid mechanics of micro-devices. The Freeman Scholar Lecture. J Fluid Eng 121:5–33
Gad-el-Hak M (2003) Comments on critical view on new results in micro-fluid mechanics. Int J Heat Mass Transfer 46:3941–3945
Gamart G, Favre-Marinet M, Asendrych D (2005) Conduction and entrance effects on laminar liquid flow and heat transfer in rectangular micro-channels. Int J Heat Mass Transfer 48:2943–2954
Gao P, Le Person S, Favre-Marinet M (2002) Scale effects on hydrodynamics and heat transfer in two-dimensional mini and micro-channels. Int J Thermal Sci 41:1017–1027
Garimella SV, Sobhan CB (2003) Transport in micro-channels – a critical review. Ann Rev Heat Transfer 13:1–50
Gnielinski V (1976) New equations for heat and mass transfer in turbulent pipe and channel flow. Int Chem Eng 16:359–368
Gruntfest J, Young JP, Johnson NL (1964) Temperatures generated by the flow of liquids in pipers. J Appl Phys 35:18–23
Gua Z-Y, Li Z-X (2003) Size effect on micro-scale single-phase flow and heat transfer. Int J Heat Mass Transfer 46:149–159
Harms TM, Kazmierzak MJ, Gerner FM (1999) Developing convective heat transfer in deep rectangular micro-channels. Int J Heat Fluid Flow 20:149–157
Hassan I, Phuttavong P, Abdelgawad M (2004) Micro-channel heat sinks: an overview of the state of the art. Microscale Thermophys Eng 8:183–204
Hehnecke DK (1968) Heat transfer by Hagen–Poiseuille flow in the thermal development region with axial conduction. Wazme Stoffubertz 1:177–184
Herwig H (2000) Flow and heat transfer in micro systems. Is everything different or just smaller. ZAMM 82:579–586
Herwig H, Hausner O (2003) Critical view on new results in micro-fluid mechanics: an example. Int J Heat Mass Transfer 46:935–937
Hetsroni G, Gurevich M, Mosyak A, Rozenblit R (2003) Surface temperature measurement of a heated capillary tube by means of an infrared technique. Meas Sci Technol 14:807–814
Hetsroni G, Gurevich M, Mosyak A, Rozenblit R (2004) Drag reduction and heat transfer of surfactants flowing in a capillary tube. Int J Heat Mass Transfer 47: 3797–3809
Hetsroni G, Mosyak A, Pogrebnyak E, Yarin LP (2005) Fluid flow in micro-channels Int J Heat Mass Transfer 48:1982–1998
Hetsroni G, Mosyak A, Segal Z (2001) Nonuniform temperature distribution in electronic devices cooled by flow in parallel micro-channels. IEEE Trans Comp Packag Technol 24(1):16–23
Ho CM, Tai Y-C (1998) Micro-electronic mechanic systems (MEMS) and fluid flows. Ann Rev Fluid Mech 30:5–33
Horiuchi K, Dutta P (2004) Joule heating effects in electroosmotically driven microchannel flows. Int J Heat Mass Transfer 47:3085–3095
Hunter RJ (1981) Zeta potential in colloid science: principles and applications. Academic, New York
Incropera FP, De Witt DP (1996) Fundamentals of heat and mass transfer, 4th edn. Wiley, New York
Judy J, Maynes D, Webb BW (2002) Characterization of friction pressure drop for liquid flows through micro-channels. Int J Heat Mass Transfer 45:3477–3489
Kandlikar S, Grande W (2002) Evolution of micro-channel flow passages – thermohydraulic performance and fabrication technology. In: Proceedings of IMEECE, ASME International Mechanical Engineering Congress and Exposition, New Orleans, November 2002, pp 1–13
Kandlikar SG, Joshi S, Tian S (2003) Effect of surface roughness on heat transfer and fluid flow characteristics at low Reynolds numbers in small diameter tubes. Heat Transfer Eng 24(3):4–16
Kays WM, Crawford ME (1993) Convective heat and mass transfer. McGraw-Hill, New York
Klein D, Hetsroni G, Mosyak A (2005) Heat transfer characteristics of water and APG surfactant solution in a micro-channel heat sink. Int J Multiphase Flow 31:393–415

Koo J, Kleinstreuer C (2004) Viscous dissipation effects in micro-tubes and micro-channels. Int J Heat Mass Transfer 47:3159–3169
Kostic M (1994) On turbulent drag and heat transfer reduction phenomena and laminar heat transfer enhancement in non-circular duct flow of certain non-Newtonian fluid. Int J Heat Mass Transfer 37:133–147
Kroeker CJ, Soliman HM, Ormiston SJ (2004) Three-dimensional thermal analysis of heat sinks with circular cooling micro-channels. Int J Heat Mass Transfer 47:4733–4744
Lee PS, Garimella SV, Liu D (2005) Investigation of heat transfer in rectangular micro-channels. Int J Heat Mass Transfer 48:1688–1704
Lelea D (2005) Some considerations on frictional losses evaluation of a water flow in micro-tubes. Int Comm Heat Mass Transfer 32:964–973
Lelea D, Nishio S, Takano K (2004) The experimental research on micro-tube heat transfer and fluid flow of distilled water. Int J Heat Mass Transfer 47:2817–2830
Li J, Peterson GP, Cheng P (2004) Three-dimensional analysis of heat transfer in a micro-heat sink with single phase flow. Int J Heat Mass Transfer 47:4215–4231
Lin TY, Yang CY (2007) An experimental investigation by method of fluid crystal thermography. Int. J. Heat Mass Transfer 50(23-24):4736-4742
Ma HB, Peterson GP (1997) Laminar friction factor in micro-scale ducts of irregular cross section. Microscale Thermophys Eng 1:253–265
Mala GM, Li D (1999) Flow characteristics of water in micro-tubes. Int J Heat Fluid Flow 20:142–148
Mala GM, Li D, Dale JD (1997a) Heat transfer and fluid flow in micro-channels. Int J Heat Mass Transfer 40:3079–3088
Mala GM, Li D, Werner C (1997b) Flow characteristics of water through a micro-channel between two parallel plates with electro kinetic effects. Int J Heat Fluid Flow 18:491–496
Male van P, Croon de MHJM, Tiggelaar RM, Derg van den A, Schouten JC (2004) Heat and mass transfer in a square micro-channel with asymmetric heating. Int J Heat Mass Transfer 47:87–99
Maranzana G, Perry I, Maillet D (2004) Mini- and micro-channels: influence of axial conduction in the walls. Int J Heat Mass Transfer 47:3993–4004
Maynes D, Webb BW (2003) Full developed electro-osmotic heat transfer in microchannels. Int J Heat Mass Transfer 46:1359–1369
Morini GL (2004) Single-phase convective heat transfer in micro-channels: overview of experimental results. Int J Thermal Sci 43:631–651
Morini GL (2005) Viscous heating in liquid flows in micro-channels. Int J Heat Mass Transfer 48:3637–3647
Nguyen NT, Bochnia D, Kiehnscherrf R, Dozel W (1996) Investigation of forced convection in micro-fluid systems. Sens Actuators A 55:49–55
Nguyen TV (1992) Laminar heat transfer for thermal developing flow in ducts. Int J Heat Mass Transfer 35:1733–1741
Owhaib W, Palm B (2004) Experimental investigation of single-phase convective heat transfer in circular micro-channels. Exp Thermal Fluid Sci 28:105–110
Peng XF, Peterson GP (1995) The effect of thermofluid and geometric parameters on convection of liquid through rectangular micro-channels. Int J Heat Mass Transfer 38:755–758
Peng XF, Peterson GP (1996) Convective heat transfer and flow friction for water flow in micro-channel structures. Int J Heat Mass Transfer 39:2599–2608
Peng XF, Wang BX, Peterson GP, Ma NB (1995) Experimental investigation of heat transfer in flat plates with rectangular micro-channels. Int J Heat Mass Transfer 38:127–137
Petukhov BS, Kurgano V, Gladuntsov A (1973) Heat transfer in turbulent pipe flow of gases with variable properties. Heat Transfer Sov Res 5:109–116
Petukhov BS (1967) Heat transfer and drag of laminar flow of liquid in pipes. Energy, Moscow
Qu W, Mala GM, Li D (2000) Heat transfer for water flow in trapezoidal silicon micro-channels. Int J Heat Mass Transfer 43:3925–3936
Qu W, Mudawar I (2002) Analysis of three-dimensional heat transfer in micro-channel heat sinks. Int J Heat Mass Transfer 45:3973–3985

Qu W, Mudawar I (2002) Experimental and numerical study of pressure drop and heat transfer in a single-phase micro-channel heat sink. Int J Heat Mass Transfer 45:2549–2565
Qu W, Mudawar I (2004) Measurement and correlation of critical heat flux in two-phase micro-channel heat sinks. Int J Heat Mass Transfer 47:2045–2059
Ren L, Qu W, Li D (2001) Interfacial electro kinetic effects on liquid flow in micro-channels. Int J Heat Mass Transfer 44:3125–3134
Reynaud S, Debray F, Frans J-P, Maitre T (2005) Hydrodynamics and heat transfer in two-dimensional mini-channels. Int J Heat Mass Transfer 48:3197–3211
Schlichting H (2000) Boundary layer theory, 8th edn. Springer, Berlin Heidelberg New York
Shah RK, London AL (1978) Laminar flow forced convection in ducts. Academic, New York
Sobhan CB, Garimella SV (2001) A comparative analysis of studies on heat transfer and fluid flow in micro-channels. Microscale Thermophys Eng 5:293–311
Tiselj I, Hetsroni G, Mavko B, Mosyak A, Pogrebhyak E, Segal Z (2004) Effect of axial conduction on the heat transfer in micro-channels. Int J Heat Mass Transfer 47:2551–2565
Toh KC, Chen XY, Chai JC (2002) Numerical computation of fluid flow and heat transfer in micro-channels. Int J Heat Mass Transfer 45:5133–5141
Tso CP, Mahulikar SP (1998) The use of the Brinkman number for single phase forced convective heat transfer in micro-channels. Int J Heat Mass Transfer 41:1759–1769
Tso CP, Mahulikar SP (1999) The role of the Brinkman number in analyzing flow transitions in micro-channels. Int J Heat Mass Transfer 42:1813–1833
Tso CP, Mahulikar SP (2000) Experimental verification of the role of the Brinkman number in micro-channels using local parameters. Int J Heat Mass Transfer 43:1837–1849
Tunc G, Bayazitoglu Y (2001) Heat transfer in micro-tubes with viscous dissipation. Int J Heat Mass Transfer 44:2395–2403
Turner SE, Sun H, Faghri M, Gregory OJ (1999) Local pressure measurement of gaseous flow through micro-channels. ASME HTD 364(3):71–80
Turner SE, Sun H, Faghri M, Gregory OJ (2000) Effect of surface roughness on gaseous flow through micro-channels. ASME HTD 366(2):291–298
Wang BX, Peng XF (1994) Experimental investigation on liquid forced-convection heat transfer through micro-channels. Int J Heat Mass Transfer 37(1):73–82
Warrier GR, Dhir VK, Momoda LA (2002) Heat transfer and pressure drop in narrow rectangular channels. Exp Thermal Fluid Sci 26:53–64
Weigand B, Lauffer D (2004) The extended Graetz problem with piecewise constant wall temperature for pipe and channel flows. Int J Heat Mass Transfer 47:5303–5312
Wu HY, Cheng P (2003) An experimental study of convective heat transfer in silicon micro-channels with different surface conditions. Int J Heat Mass Transfer 46:2547–2556
Wu PY, Little WA (1984) Measuring of the heat transfer characteristics of gas flow in fine channel heat exchangers for micro-miniature refrigerators. Cryogenics 24:415–420
Yang C, Li D (1998) Analysis of electro kinetic effects on the liquid flow in micro-channels. Coll Surf A Physicochem Eng Aspects 143:339–353
Yang CY, Lin TY (2007) Heat transfer characteristics of water flow in micro-tubes. Exp. Thermal and Fluid Science 32:432-439
Yoo JY (2006) Recent studies of fluid flow and heat transfer in thermal micro-devices. Nanoscale Microscale Thermophys Eng 10:67–81
Zel'dovich YaB, Barenblatt GI, Librovich VB, Maxhviladse GM (1985) Mathematical theory of combustion and explosion. Plenum, New York
Zhao CY, Lu TJ (2002) Analysis of micro-channels for electronic cooling. Int J Heat Mass Transfer 45:4857–4869

Nomenclature

A	Cross-section
A_d	Ratio of convective heat transfer to dissipation one
a	Relative surface roughness
c_p	Specific heat
C	Concentration
d	Inner diameter
d_h	Hydraulic diameter
h	Heat transfer coefficient, enthalpy
H	Micro-channel height
I_0	Bessel function
i_e	Current density
k	Thermal conductivity
k_s	Average height of roughness
L	Length
M	Conductive to convective heat flux ratio
m	Flow rate
Ma	Mach number
N	Power
P	Pressure
q	Heat flux
Re_sh	Shear Reynolds number, based on the shear viscosity
r	Radius
r_0	Tube radius, inner hydraulic radius
R	Gas constant, $R = r/r_0$ dimensionless distance from tube axis
s	Volumetric energy generation
T	Temperature
$\overline{T}$	Average fluid temperature
U	Average velocity
U_m	Normalized local velocity
u	Streamwise velocity
u_max	Maximum possible electro-osmotic velocity
v	Spanwise velocity
W	Channel width
W_b	Width of the channel bottom
W_c	Spacing
W_t	Width of the channel top
x	Longitudinal coordinate
$\mathrm{Br} = \dfrac{\mu U^2}{k(T_\mathrm{w} - T_\mathrm{f})}$	Brinkman number
$\mathrm{Ec} = \dfrac{U^2}{2c_\mathrm{p}\Delta\mathrm{T}}$	Eckert number

$\mathrm{Kn} = \dfrac{\overline{\lambda}}{d_\mathrm{h}}$	Knudsen number
$\mathrm{Na} = -\dfrac{4\beta\mu U^2}{k}$	Nahme number
$\mathrm{Nu} = \dfrac{hd_\mathrm{h}}{k_\mathrm{f}}$	Nusselt number
Nu_0	Nusselt number corresponds to negligible viscous dissipation
$\mathrm{Pe} = \dfrac{Ud_\mathrm{h}}{\alpha}$	Peclet number
$\mathrm{Pr} = \dfrac{\nu}{\alpha}$	Prandtl number
$\mathrm{Re} = \dfrac{Ud_\mathrm{h}}{\nu}$	Reynolds number
$X^+ = \dfrac{x}{d_\mathrm{h}\mathrm{Pe}}$	Dimensionless longitudinal coordinate

Greek symbols

α	Thermal diffusivity
β	Temperature sensitivity
$\Delta T = T_\mathrm{w} - T_\mathrm{f}$	Temperature difference
δ	Thickness of tube
γ	Aspect ratio, relation of $c_\mathrm{p}/c_\mathrm{v}$
ε	Fluid dielectric constant
ζ	Wall zeta potential
θ	Dimensionless temperature
λ	Friction factor, Debye length
$\overline{\lambda}$	Mean free path
μ	Dynamic viscosity
ν	Kinematic viscosity
Π	Bejan number
ρ	Density
σ	Liquid electrical resistivity
Φ	Applied potential field
ψ	Excess charge distribution

Subscripts

ad	Adiabatic
av	Average

ax	Axial
b	Bulk
cond	Conduction
conv	Convection
d	Developed
f	Fluid
h	Heated
in	Inner, inlet
inv	Inversion
out	Outer, outlet
sh	Shear
sur	Surfactant
stg	Stagnation
th	Theoretical
therm	Thermal
tot	Total
v	Volume
w	Wall
wat	Water
1	Fluid
2	Wall
2.1	Ratio parameter of wall to fluid